



CERN-EP-2024-193
12 July 2024

Measurement of beauty production via non-prompt charm hadrons in p–Pb collisions at $\sqrt{s_{NN}} = 5.02$ TeV

ALICE Collaboration*

Abstract

The production cross sections of D^0 , D^+ , and Λ_c^+ hadrons originating from beauty-hadron decays (i.e. non-prompt) were measured for the first time at midrapidity in proton–lead (p–Pb) collisions at the center-of-mass energy per nucleon pair of $\sqrt{s_{NN}} = 5.02$ TeV. Nuclear modification factors (R_{pPb}) of non-prompt D^0 , D^+ , and Λ_c^+ are calculated as a function of the transverse momentum (p_T) to investigate the modification of the momentum spectra measured in p–Pb collisions with respect to those measured in proton–proton (pp) collisions at the same energy. The R_{pPb} measurements are compatible with unity and with the measurements in the prompt charm sector, and do not show a significant p_T dependence. The p_T -integrated cross sections and p_T -integrated R_{pPb} of non-prompt D^0 and D^+ mesons are also computed by extrapolating the visible cross sections down to $p_T = 0$. The non-prompt D-meson R_{pPb} integrated over p_T is compatible with unity and with model calculations implementing modification of the parton distribution functions of nucleons bound in nuclei with respect to free nucleons. The non-prompt Λ_c^+/D^0 and D^+/D^0 production ratios are computed to investigate hadronisation mechanisms of beauty quarks into mesons and baryons. The measured ratios as a function of p_T display a similar trend to that measured for charm hadrons in the same collision system.

1 Introduction

Measurements of heavy-flavour hadron production in hadronic collisions provide crucial tests for calculations based on quantum chromodynamics (QCD). Due to their large masses with respect to the QCD energy scale, heavy quarks (i.e. charm and beauty) are primarily produced at the early stages of the collision via hard-scattering processes with large momentum transfer, legitimising the calculations of inclusive production cross sections via perturbative QCD (pQCD). These calculations rely on a factorisation scheme where the p_T -differential production cross sections of charm or beauty hadrons are calculated as a convolution of three terms: (i) the parton distribution functions (PDFs) of the incoming nucleons, which describe the Bjorken- x distributions of quarks and gluons within the incoming hadrons, (ii) the partonic scattering cross section, calculated as a perturbative series in powers of the strong coupling constant α_s , and (iii) the fragmentation function parametrising the non-perturbative evolution of a heavy quark into a given heavy-flavour hadron species. The fragmentation functions are determined from measurements in e^+e^- collisions [1] and used to compute the production cross section in hadronic collisions, under the assumption that the relevant hadronisation processes are “universal”, i.e. independent of the collision energy and system.

To isolate the effects of hadronisation, heavy-flavour hadron-to-hadron production yield ratios are especially effective, since the PDFs and the partonic interaction cross sections are common to all charm or beauty hadron species and their effects cancel out in the yield ratios when using the factorisation approach. Measurements of non-strange charm and beauty-meson production cross sections in pp and p–Pb collisions at the LHC [2–12] show that the meson-to-meson ratios are described by the pQCD calculations at next-to-leading order accuracy with all-order resummation of next-to-leading logarithms, such as FONLL [13, 14] and GM-VFNS [15–18], and by PYTHIA 8 event generator using the Monash tune [19, 20], which is tuned on e^+e^- collisions. However, all these calculations largely underpredict the production of charm and beauty baryons [21–24]. In addition, charm and beauty baryon-to-meson yield ratios, measured at mid- and forward rapidity at the LHC, show significant deviations from the values measured in e^+e^- collisions [21, 22, 24–36], indicating that the assumption of universality of the hadronisation process across collision systems might no longer be valid at the LHC [6, 14, 37]. The reconstruction of prompt charm hadrons, which are produced from the decay of excited charm states or from charm-quark hadronisation, and of non-prompt charm hadrons, which stem from the decay of beauty hadrons, provides a good approach for probing the distinct sectors of charm and beauty. The prompt charm baryon-to-meson production ratios were measured in p–Pb collisions by the LHCb Collaboration at both forward ($1.5 < y_{\text{lab}} < 4.0$ in the laboratory-frame) and backward ($-5.0 < y_{\text{lab}} < -2.5$) rapidity regions [32, 38]. Comparatively, these findings indicate an augmented baryon-to-meson yield ratios measured at forward/backward rapidity with respect to the corresponding measurements in e^+e^- and ep collisions, although this is smaller compared to the enhancement observed when considering midrapidity measurements [22, 26, 29]. In the beauty sector, the ALICE Collaboration measured production cross sections of non-prompt D^0 and Λ_c^+ hadrons at midrapidity ($|y| < 0.5$) in pp collisions at $\sqrt{s} = 13$ TeV [36]. The measured baryon-to-meson production ratio shows an enhancement similar to that observed in the charm sector, and the enhancement at midrapidity is similar to the one observed at forward rapidity by the LHCb Collaboration measuring the Λ_b^0 -baryon production relative to that of B mesons in pp and p–Pb collisions [24, 33–35]. Modification of charm and beauty baryon-to-meson ratios from e^+e^- to pp and p–Pb collisions suggests the influence of the hadronic or partonic environment on the hadronisation process [39]. Further hadronisation effects, apart from pure in-vacuum fragmentation, like recombination (or coalescence) of charm quarks with quarks or di-quarks from a thermal medium [40–43], statistical hadronisation including contributions from undiscovered higher-mass resonant states [44–46], and string formation beyond the leading-colour approximation [47, 48], serve as examples of implementations considered by theorists to refine the modelling of hadronisation to baryons.

Measurements of heavy-flavour hadron production in proton–nucleus collisions also allow to study var-

ious effects related to the presence of nuclei in the colliding system, denoted as cold-nuclear-matter (CNM) effects. In the initial state of the collisions, the PDFs of inbound nucleons are modified by the nuclear environment as compared to free nucleons, depending on the parton momentum fraction x , the squared momentum transfer Q^2 in the hard scattering processes, and the nucleus mass number A [49, 50]. At LHC energies and midrapidity ($|y_{\text{lab}}| < 0.5$), the most relevant effect on the PDF is called shadowing. It corresponds to a reduction of the parton densities at x lower than 10^{-2} , which becomes stronger when Q^2 decreases and the nucleus mass number A increases. This effect, induced by the high phase-space density of small- x partons [51–54], can be described within the factorisation scheme by means of phenomenological parametrisations, denoted as nuclear PDFs (nPDFs). The modification of the small- x parton dynamics can significantly reduce the charm and beauty hadron yield with respect to pp collisions at low p_T . Furthermore, multiple scattering of partons in the nucleus can modify the kinematic distribution of the produced hadrons. Partons can lose energy in the initial stages of the collision via initial-state radiation [55] or experience transverse momentum broadening due to multiple soft collisions before the heavy-quark pair is produced [56, 57]. These initial-state effects are expected to have an influence on charm-hadron production at low and intermediate p_T ($p_T < 4 \text{ GeV}/c$). For this reason, measurements of the charm- and beauty-hadron production cross section and its nuclear modification factor R_{pPb} , which is defined as the ratio of the production cross section in p–Pb to that in pp collisions scaled by the mass number of the Pb nucleus (A_{Pb}), down to low p_T could provide important information, helping to significantly reduce the uncertainties on the gluon nPDFs at small x [58, 59].

In addition to the aforementioned initial-state effects, final-state effects may also be responsible for modifications of heavy-flavour hadron yields and momentum distributions. Measurements in the light- and heavy-flavour sectors in high-multiplicity pp and p–Pb collisions at different collision energies showed significant flow-like effects [21, 60, 61]. These effects resemble those observed in high-energy nucleus–nucleus collisions and are ascribed to quark–gluon plasma formation. In this picture, particles of larger mass are boosted to higher transverse momenta due to a common velocity field [62]. However, baryon production at intermediate p_T may also be enhanced as a result of hadronisation via quark recombination [63].

The ALICE and CMS Collaborations measured the R_{pPb} of D and B meson in p–Pb collisions, finding values close to unity within the rapidity ranges $|y_{\text{lab}}| < 0.5$ [64] and $|y_{\text{lab}}| < 2.4$ [65], respectively. In contrast, the LHCb Collaboration measurements at forward ($2.5 < y_{\text{lab}} < 3.5$) and backward rapidity ($-3.5 < y_{\text{lab}} < -2.5$) [35], evidence a suppression of up to 20% for beauty mesons in the forward rapidity interval and no significant suppression in the backward rapidity interval. Model calculations based on nPDFs describe well these observations.

In the baryon sector, the ALICE Collaboration found that the Λ_c^+ R_{pPb} depends on p_T , being below unity at low p_T and above unity at high p_T [26]. Simulations based on POWHEG+PYTHIA 6 [66, 67], combined with EPPS16 nPDF [54], reproduce the results at low p_T but do not describe the measured trend at intermediate p_T . The Λ_b^0 measurements in p–Pb collisions at large rapidities by the LHCb Collaboration are consistent with the corresponding measurements in pp collisions within uncertainties [35].

In this article, possible effects related to the modification of hadronisation mechanisms, and initial and final-state effects at midrapidity ($|y_{\text{lab}}| < 0.5$) in p–Pb collisions in the beauty sector are investigated. The p_T -differential production cross sections and nuclear modification factors of non-prompt D^0 , D^+ , and Λ_c^+ hadrons in p–Pb collisions at $\sqrt{s_{\text{NN}}} = 5.02 \text{ TeV}$ are reported. The D^0 meson is reconstructed in the interval $1 < p_T < 24 \text{ GeV}/c$, while the D^+ and Λ_c^+ hadrons are reconstructed in the interval $2 < p_T < 24 \text{ GeV}/c$. By integrating the p_T -differential results and extrapolating to $p_T = 0$ using pQCD calculations, the p_T -integrated non-prompt D^0 and D^+ production cross sections are computed. The paper is organised as follows. Section 2 describes the ALICE apparatus and the analysed data samples. Section 3 details the analysis methods used and outlines the corrections applied to calculate the p_T -differential production cross sections. Section 4 describes the sources of systematic uncertainty. The

results are presented in Section 5. Finally, a summary is given in Section 6.

2 Experimental setup and data sample

The ALICE apparatus [68] consists of a set of detectors for particle reconstruction and identification at midrapidity ($|\eta| < 0.9$) embedded in a solenoidal magnet, a forward ($-4 < \eta < -2.5$) muon spectrometer, and a set of forward and backward detectors for triggering and event characterisation. Typical detector performance in pp, p–Pb, and Pb–Pb collisions is presented in [69]. The reconstruction of heavy-flavour hadrons from their hadronic decay products at midrapidity primarily relies on the Inner Tracking System (ITS) [70], the Time Projection Chamber (TPC) [71], and the Time-Of-Flight detector (TOF) [72] for tracking, primary and decay vertex reconstruction, and charged-particle identification (PID). The V0 detector arrays [73] are used for triggering and event selection.

The data sample used in this analysis are from proton–lead collisions at $\sqrt{s_{\text{NN}}} = 5.02$ TeV collected in 2016. The events were recorded with a minimum-bias (MB) interaction trigger that required coincident signals in both scintillator arrays of the V0 detector, which covers the full azimuth in the pseudorapidity intervals $-3.7 < \eta < -1.7$ and $2.8 < \eta < 5.1$. The V0 timing information was used together with that from the Zero-Degree Calorimeter (ZDC) [69] for offline rejection of beam-beam or beam-gas interactions occurring outside the nominal colliding bunches.

To ensure uniform acceptance in pseudorapidity, events were required to have a reconstructed collision vertex located within ± 10 cm from the nominal collision point along the beam-line direction. Events composed of several interactions per bunch crossing, whose probability was below 0.5%, were rejected using an algorithm based on track segments, defined within the two innermost ITS layers, to detect multiple interaction vertices [69]. The influence of potentially remaining pile-up events is on the percent level and does not have an impact on the final results of the presented analysis. After these selections, the data sample consisted of about 600 million events, corresponding to an integrated luminosity $\mathcal{L}_{\text{int}} = 292 \pm 11 \mu\text{b}^{-1}$ [74]. During the p–Pb data taking period, the beam energies were 4 TeV for protons and 1.58 TeV per nucleon for lead nuclei. With this beam configuration, the nucleon–nucleon center-of-mass system moves in rapidity by $\Delta y_{\text{cms}} = 0.465$ in the direction of the proton beam. The charm-hadron analyses were performed in the laboratory-frame interval $|y_{\text{lab}}| < 0.5$, leading to a shifted center-of-mass rapidity coverage of $-0.96 < y_{\text{cms}} < 0.04$.

3 Analysis technique

3.1 Non-prompt D^0 , D^+ , and Λ_c^+ raw yields

The D^0 , D^+ , and Λ_c^+ charm hadrons, along with their charge conjugates, were reconstructed via the following hadronic decay channels: $D^0 \rightarrow K^- \pi^+$ with branching ratio $\text{BR} = (3.95 \pm 0.03)\%$, $D^+ \rightarrow \pi^+ K^- \pi^+$ with $\text{BR} = (9.38 \pm 0.16)\%$, $\Lambda_c^+ \rightarrow p K^- \pi^+$ with $\text{BR} = (6.28 \pm 0.32)\%$, and $\Lambda_c^+ \rightarrow p K_S^0$ with $\text{BR} = (1.59 \pm 0.08)\%$, followed by $K_S^0 \rightarrow \pi^+ \pi^-$ with $\text{BR} = (69.20 \pm 0.05)\%$ [75]. The D^0 -, D^+ -, and Λ_c^+ -hadron candidates were defined by combining pairs or triplets of tracks reconstructed with the proper charge sign. While for the $\Lambda_c^+ \rightarrow p K_S^0$ candidates, the V-shaped decay of the K_S^0 meson into two pion-track candidates was combined with a proton-track candidate using a Kalman-Filter vertexing algorithm [76], as described in [21]. All daughter tracks were required to be reconstructed within $|\eta| < 0.8$, with at least 70 associated space points in the TPC, $\chi^2/\text{ndf} < 2$ of the fit quality of the TPC tracks (where ndf is the number of degrees of freedom involved in the track fit procedure), and a minimum of 2 (out of 6) reconstructed clusters in the ITS, with at least one in either of the two innermost layers. These track-selection criteria reduce the D-meson and Λ_c^+ -baryon acceptance in rapidity, which drops steeply to zero for $|y_{\text{lab}}| > 0.5$ at low p_{T} and for $|y_{\text{lab}}| > 0.8$ at high p_{T} . Therefore, a p_{T} -dependent fiducial acceptance region $|y_{\text{lab}}| < y_{\text{fid}}(p_{\text{T}})$ was applied to grant a uniform acceptance in the considered rapidity range. The

$y_{\text{fid}}(p_{\text{T}})$ was defined as a second-order polynomial function, increasing from 0.5 to 0.8 in the transverse momentum range $0 < p_{\text{T}} < 5 \text{ GeV}/c$, and as a constant term, $y_{\text{fid}} = 0.8$, for $p_{\text{T}} > 5 \text{ GeV}/c$.

The D^0 , D^+ , and Λ_c^+ decay weakly with a mean proper decay length ($c\tau$) of about 123, 312, and 60 μm , respectively [75]. Charm hadrons coming from beauty-hadron decays are even more displaced from the primary vertex since their estimated $c\tau$ is about 500 μm , as for beauty hadrons. Therefore, these analyses were based on the reconstruction of decay-vertex topologies displaced from the primary vertex and, according to the selection applied, it is possible not only to separate candidates from the combinatorial background, but also the contributions of prompt and non-prompt charm hadrons.

To reduce the large combinatorial background and to separate the contributions of prompt and non-prompt charm hadrons, a machine-learning approach with multi-class classification, based on Boosted Decision Trees (BDT), implemented in the XGBoost library [77, 78], was adopted. For the BDT training, signal samples of prompt and non-prompt charm hadrons were obtained from simulations using the PYTHIA 8 event generator [19] (Monash-13 tune [20]), embedded in an underlying p–Pb collision generated with HIJING 1.36 [79], to describe better the charged-particle multiplicity and detector occupancy observed in the data. Background samples were extracted from candidate invariant-mass distributions within the range of $5\sigma < |\Delta M| < 9\sigma$ in the data, where ΔM represents the difference between the candidate invariant mass and the nominal mass of the hadron candidate, and σ represents the invariant-mass resolution.

Before the training, loose selections were applied based on the decay kinematics and topologies along with the PID information of the decay-product tracks. The PID selections were based on the difference between the measured and expected detector signals for a given particle species hypothesis, in units of the detector resolution (n_{σ}^{det}). Protons, pions, and kaons were selected by requiring compatibility with the respective hypothesis within three standard deviations (3σ) for both the TPC specific energy loss and the TOF time-of-flight. For tracks without a measured signal in the TOF, the PID selections relied only on information from the TPC.

Independent BDT models were trained for each p_{T} interval of the analysis of each D-meson species and the two Λ_c^+ decay channels using different variables related to the displaced decay-vertex topology and the PID information of the decay tracks. The main variables used were (i) the distance of closest approach between the reconstructed tracks and the primary vertex, (ii) the distance between the charm-hadron decay vertex and the primary vertex, (iii) the charm-hadron impact parameter, (iv) the cosine of the pointing angle between the charm-hadron candidate line-of-flight and its reconstructed momentum. In the case of the $\Lambda_c^+ \rightarrow \text{pK}_S^0$ decay, additional training variables related to the decay topology of the K_S^0 and Λ_c^+ were used as in [21]. The three BDT output scores are related to the candidate probability of being a prompt charm hadron, a non-prompt charm hadron, or combinatorial background. Selections on the non-prompt and combinatorial background BDT scores, corresponding to a requirement of a low probability for a candidate to be combinatorial background and a high probability to be non-prompt, were optimised to obtain a high non-prompt charm-hadron fraction in the inclusive signals while maintaining a reliable signal extraction, meaning a statistical significance larger than 3, as done in [2, 80].

The raw yields of D^0 , D^+ , and Λ_c^+ hadrons, including particles and antiparticles, were extracted via binned maximum-likelihood fits to the invariant-mass (M) distributions of the selected charm-hadron candidates. The raw yields were extracted in transverse-momentum intervals in the range $1 < p_{\text{T}} < 24 \text{ GeV}/c$ for D^0 mesons, and $2 < p_{\text{T}} < 24 \text{ GeV}/c$ for D^+ mesons and Λ_c^+ baryons. The fitting function was composed of an exponential or polynomial term for describing the background and a Gaussian term for the signal. To improve the stability of the fits, the widths of the charm-hadron signal peaks were fixed to the values extracted from data samples enhanced with prompt candidates, given the naturally larger abundance of prompt compared to non-prompt charm hadrons. As part of the systematic uncertainty analysis, the width parameter was varied to determine its impact on the systematic uncertainty associated

with the raw-yield extraction. For the D^0 mesons, the contribution of signal candidates to the invariant-mass distribution with the wrong mass assigned to the D^0 -decay tracks, referred to as reflections, was included in the fit, and estimated as explained in [80]. The contribution of reflections to the raw yield is about 1–2%, depending on p_T . Examples of invariant-mass distributions together with the result of the fits and the estimated non-prompt fractions ($f_{\text{non-prompt}}^{\text{raw}}$) are reported in Fig. 1, for the $3 < p_T < 4$ GeV/c, $5 < p_T < 6$ GeV/c, and $4 < p_T < 8$ GeV/c intervals of the D^0 , D^+ , and Λ_c^+ hadrons, respectively.

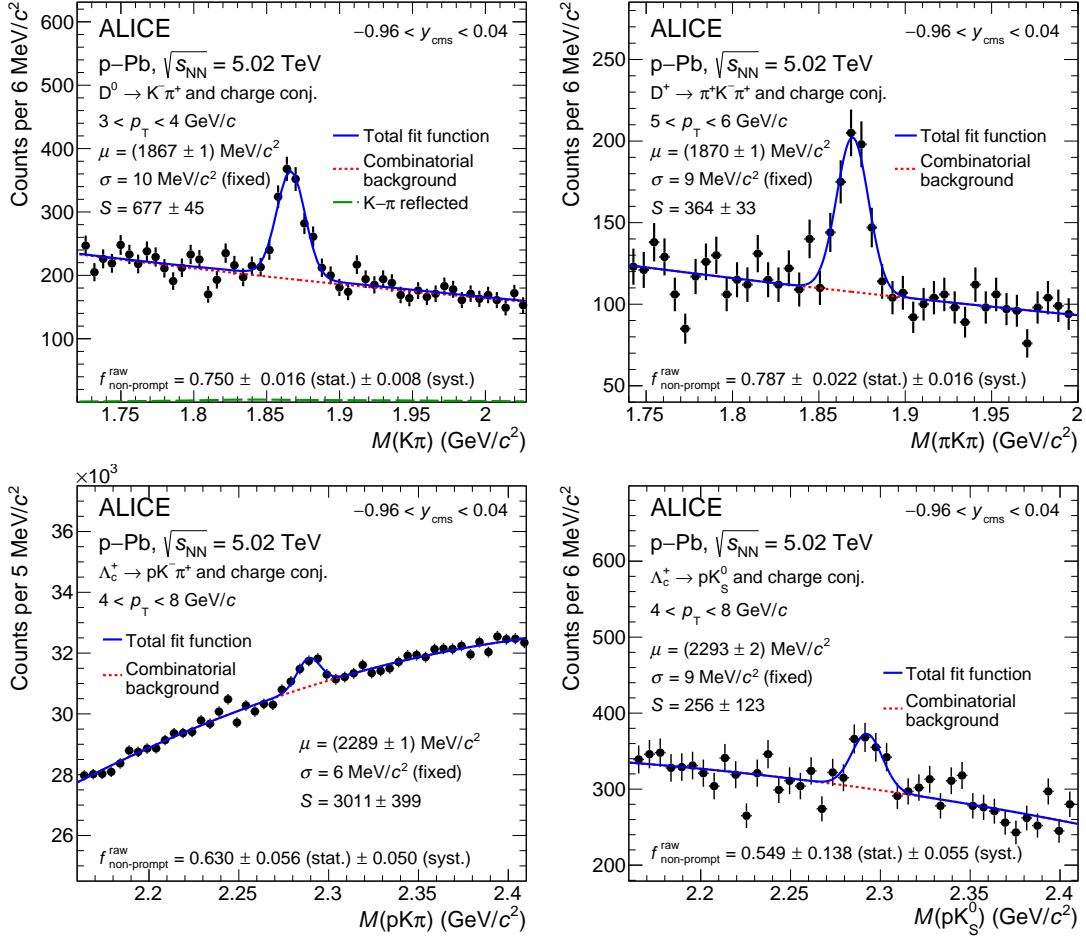


Figure 1: Invariant-mass distributions of D^0 -, D^+ -, and Λ_c^+ -hadron candidates, and their charge conjugates in selected p_T intervals. The blue solid lines show the total fit functions as described in the text and the red dashed lines show the fit function describing the combinatorial background. For D^0 -meson candidates, the solid green line represents the contribution of the reflections. The mean (μ) and fixed standard deviation (σ) of the signal fit function, along with the raw-yield (S) values, are reported together with their statistical uncertainties resulting from the fit. The fraction of non-prompt candidates in the measured raw yield ($f_{\text{non-prompt}}^{\text{raw}}$) is reported with its statistical and systematic uncertainties.

3.2 Yield corrections and non-prompt fraction estimations

The p_T -differential production cross sections of non-prompt D^0 , D^+ , and Λ_c^+ hadrons at midrapidity were computed as:

$$\left. \frac{d^2\sigma_{H_c}}{dp_T dy} \right|_{|y_{\text{lab}}| < 0.5} = \frac{1}{2} \times \frac{f_{\text{non-prompt}}^{\text{raw}}(p_T) \times N_{H_c + \bar{H}_c, \text{raw}}(p_T) \Big|_{|y_{\text{lab}}| < y_{\text{fid}}(p_T)}}{\Delta p_T \times c_{\Delta y}(p_T) \times (\text{Acc} \times \varepsilon)^{\text{non-prompt}}(p_T)} \frac{1}{\text{BR} \times \mathcal{L}_{\text{int}}}, \quad (1)$$

where $N^{\text{H}_c + \bar{\text{H}}_c, \text{raw}}$ (sum of particles and antiparticles) represents the raw yields extracted in each p_T interval, and the factor 1/2 is included to account that the raw yields contain both particles and antiparticles, while the production cross sections are given as an average of particles and antiparticles. The $f_{\text{non-prompt}}^{\text{raw}}$ factor represents the raw non-prompt fraction needed to account for the residual contribution of prompt charm hadrons in the extracted non-prompt raw yields. In addition, the yields were further divided by the width of the p_T interval (Δp_T), the correction factor for the rapidity coverage $c_{\Delta y}$, computed as the ratio between the generated hadron yield in $\Delta y = 2y_{\text{fid}}$ and that in $|y_{\text{lab}}| < 0.5$, as explained in [64], as well as the acceptance times efficiency of non-prompt charm hadrons $(\text{Acc} \times \varepsilon)^{\text{non-prompt}}$, the BR of the decay channel, and the integrated luminosity \mathcal{L}_{int} .

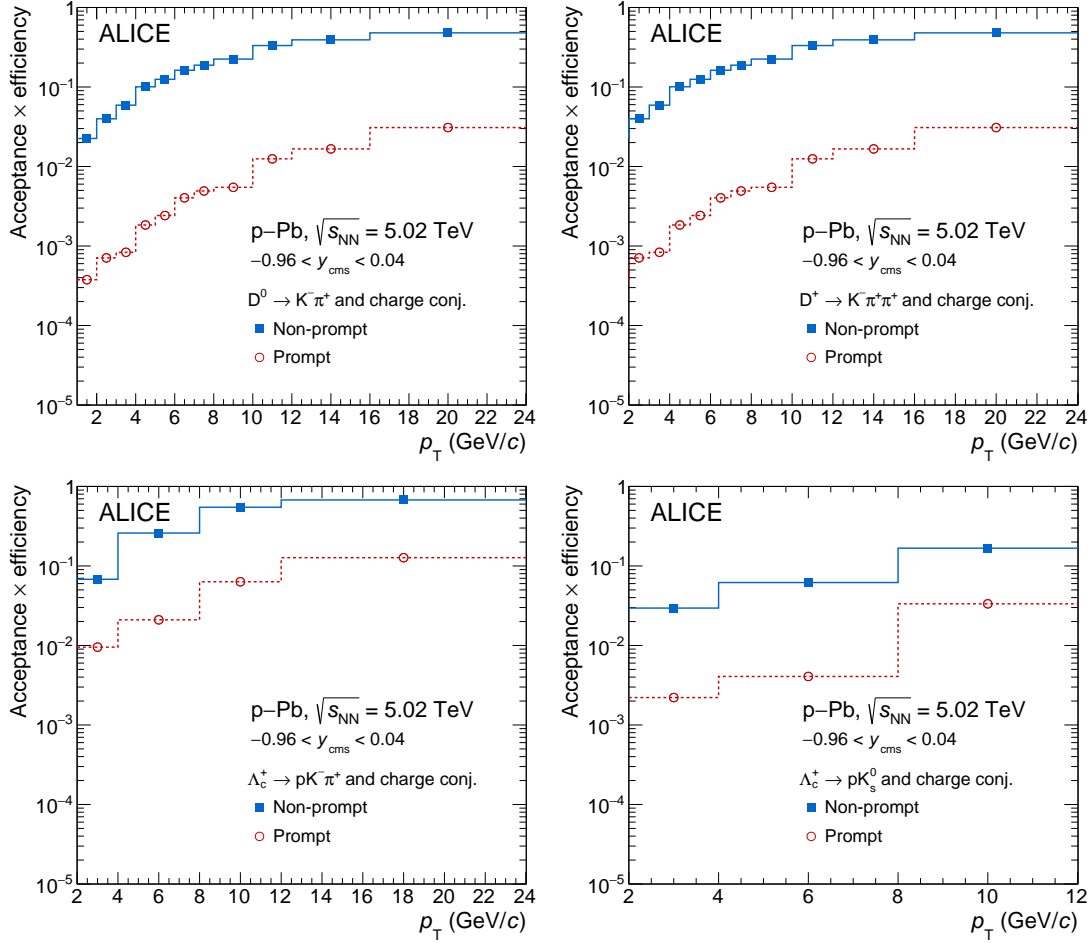


Figure 2: Acceptance-times-efficiency factors for D^0 , D^+ , and Λ_c^+ hadrons as a function of p_T .

Possible differences in the p_T shape of prompt and non-prompt charm hadrons between data and Monte Carlo (MC) simulations were corrected by weighting the simulated p_T distribution of prompt charm hadrons and of the beauty-hadron parent, respectively. For D mesons, the weights were computed by dividing the p_T spectrum predicted by FONLL calculations and the one obtained from PYTHIA 8 simulations. The FONLL p_T spectra of prompt and non-prompt D mesons in p–Pb collisions were computed using the predictions in pp collisions at $\sqrt{s} = 5.02$ TeV [13, 81], assuming that the R_{pPb} of D and B mesons are compatible with unity, in the rapidity range of this study. This assumption is based on the D-meson R_{pPb} measurements at $\sqrt{s_{\text{NN}}} = 5.02$ TeV at midrapidity by the ALICE Collaboration [64] and B-meson R_{pPb} measurements at $\sqrt{s_{\text{NN}}} = 8.16$ TeV at forward/backward rapidity by the LHCb Collaboration [35], that are in agreement with models that predict B-meson R_{pPb} values compatible with unity at midrapidity, within the theoretical uncertainties. The energy dependence of the R_{pPb} measurement is neglected. The procedure to compute the p_T spectrum based on FONLL calculations for the prompt Λ_c^+

(Λ_b^0) hadrons takes into account three essential components: the FONLL predicted p_T distribution for prompt D^0 (B) mesons in pp collisions at $\sqrt{s} = 5.02$ TeV, the prompt Λ_c^+/D^0 (Λ_b^0/B^0) ratio [21, 33] in the same collision system and energy, and the prompt $\Lambda_c^+ R_{pPb}$ at $\sqrt{s_{NN}} = 5.02$ TeV measured by the ALICE Collaboration [21]. The weights on prompt Λ_c^+ (Λ_b^0) p_T shape were derived as the product of these three components divided by the prompt Λ_c^+ (Λ_b^0) MC p_T distribution from PYTHIA 8. In addition, the weights on non-prompt Λ_c^+ were derived from Λ_b^0 based on the p_T correlation between Λ_b^0 and non-prompt Λ_c^+ from Λ_b^0 decays simulated by PYTHIA 8.

The $(\text{Acc} \times \varepsilon)$ correction was obtained from simulations, as described in Section 3.1, using samples not employed for the BDT training. The $(\text{Acc} \times \varepsilon)$ factors, computed for non-prompt D^0 , D^+ , and Λ_c^+ hadrons as a function of p_T , after applying all the selections, are shown in Fig. 2. The selection applied to obtain the non-prompt enhanced samples strongly suppresses the prompt charm-hadron efficiency. The prompt charm-hadron acceptance-times-efficiency $(\text{Acc} \times \varepsilon)$ is smaller than the non-prompt one by factors varying from 20 to 60 for D mesons and 5 to 13 for Λ_c^+ baryons, depending on the p_T interval.

A data-driven procedure, based on the construction of data samples with different abundances of prompt and non-prompt candidates, was used to estimate the fraction $f_{\text{non-prompt}}^{\text{raw}}$ of non-prompt D^0 , D^+ , and Λ_c^+ hadrons in the extracted yields. Let $i \in \{1; n\}$ designate a set among $n \in \mathbb{N}$ selection sets. Each set of BDT selection i is associated with an extracted raw-yields value (Y_i), which relates to the corrected yield of prompt (N_{prompt}) and non-prompt ($N_{\text{non-prompt}}$) charm hadrons via the corresponding prompt $(\text{Acc} \times \varepsilon)_i^{\text{prompt}}$ and non-prompt $(\text{Acc} \times \varepsilon)_i^{\text{non-prompt}}$ efficiency as follows:

$$(\text{Acc} \times \varepsilon)_i^{\text{prompt}} \times N_{\text{prompt}} + (\text{Acc} \times \varepsilon)_i^{\text{non-prompt}} \times N_{\text{non-prompt}} - Y_i = \delta_i, \quad (2)$$

where δ_i represents a residual that accounts for the equation not holding precisely due to the uncertainties of Y_i , $(\text{Acc} \times \varepsilon)_i^{\text{non-prompt}}$, and $(\text{Acc} \times \varepsilon)_i^{\text{prompt}}$. In the case of $n \geq 2$ sets, a χ^2 function can be defined based on Eq. 2, which can be minimised to obtain N_{prompt} and $N_{\text{non-prompt}}$ as explained in [2, 36].

Figure 3 shows an example of the raw-yield distribution as a function of the BDT-based selection employed in the minimisation procedure for D^0 mesons in $3 < p_T < 4$ GeV/c (left panel). The leftmost data point of the distribution is the raw yield corresponding to the looser selections on the BDT outputs related to the candidate probability of being a non-prompt charm hadron. In contrast, the rightmost one corresponds to the tightest selections. The right panel shows the p_T distributions of the raw non-prompt fraction $f_{\text{non-prompt}}^{\text{raw}}$ obtained for the set of selection criteria adopted in the analysis for non-prompt D^0 , D^+ , $\Lambda_c^+ \rightarrow pK^- \pi^+$, and $\Lambda_c^+ \rightarrow pK_S^0$. The fraction $f_{\text{non-prompt}}^{\text{raw}}$ of D^0 , D^+ , and Λ_c^+ hadrons ranges from 42 to 90% depending on the decay channel and the p_T interval.

4 Systematic uncertainties

The measurement of the p_T -differential production cross section of non-prompt charm hadrons was affected by the following sources of systematic uncertainties: (i) extraction of the raw yield from the invariant-mass distribution, (ii) non-prompt fraction estimation, (iii) corrections to the generated p_T shape in simulations, (iv) charm-hadron selection efficiency, and (v) track-reconstruction efficiency. The systematic uncertainties of the PID selection efficiency were found to be negligible, as observed in prompt charm hadron measurements [21, 64]. In addition, the p_T -differential production cross section was affected by the uncertainties on the branching ratios of the considered charm-hadron decays [75] and a systematic uncertainty on the overall normalisation induced by the uncertainties on the integrated luminosity of 3.7% [74]. The values of the systematic uncertainties for some representative p_T intervals were summarised in Table 1. The contributions of the different sources were considered to be uncorrelated and were summed in quadrature to obtain the total systematic uncertainty.

The systematic uncertainty on the raw yield extraction was evaluated for each charm-hadron species by

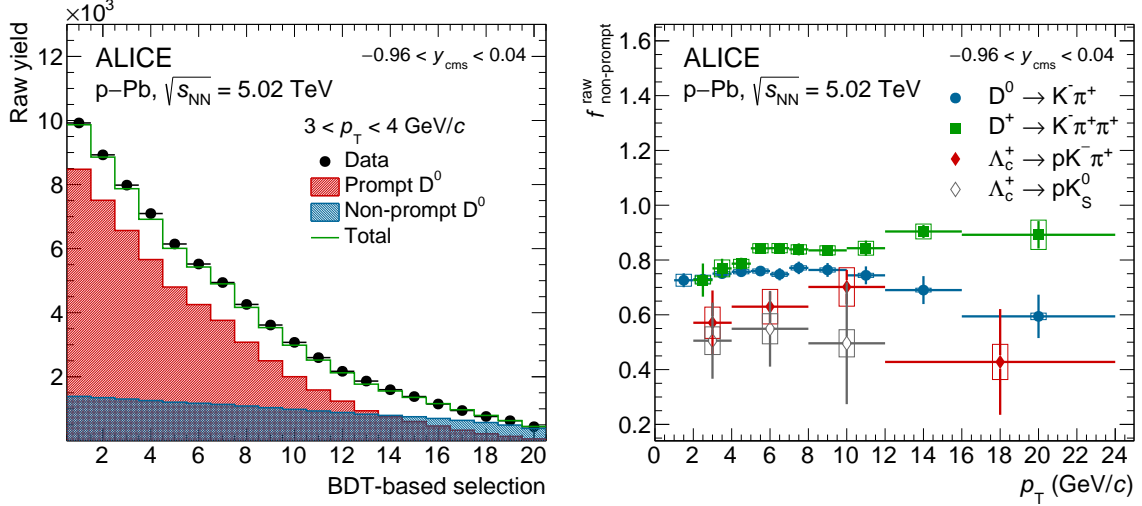


Figure 3: Left panel: example of raw-yield distribution as a function of the BDT-based selection employed in the data-driven procedure adopted to determine $f_{\text{non-prompt}}^{\text{raw}}$ of D^0 mesons. Right panel: $f_{\text{non-prompt}}^{\text{raw}}$ fractions as a function of p_T obtained for the set of selection criteria adopted in the analysis for non-prompt D^0 , D^+ , $\Lambda_c^+ \rightarrow pK^-\pi^+$, and $\Lambda_c^+ \rightarrow pK_S^0$. The vertical bars and empty boxes represent the statistical and systematic uncertainties, respectively.

Table 1: Summary of the relative systematic uncertainties on the measurement of non-prompt D^0 , D^+ , and Λ_c^+ production cross sections in different p_T intervals.

Hadron p_T (GeV/c)	$D^0 (\rightarrow K^-\pi^+)$		$D^+ (\rightarrow \pi^+K^-\pi^+)$		$\Lambda_c^+ (\rightarrow pK^-\pi^+)$		$\Lambda_c^+ (\rightarrow pK_S^0)$	
	1–2	10–12	2–3	10–12	2–4	12–24	2–4	8–12
Signal yield	3%	2%	6%	5%	7%	15%	10%	9%
Fraction estimation	3%	1%	2%	3%	10%	15%	10%	10%
p_T shape in MC	7%	0%	1%	0%	5%	0%	5%	0%
Selection efficiency	5%	4%	6%	3%	8%	8%	7%	7%
Tracking efficiency	2.0%	2.5%	3.7%	4.0%	6.0%	6.0%	5.0%	5.0%
Branching ratio [75]	0.8%		1.7%		5.1%		5.0%	
Luminosity [74]	3.7%							

repeating the fits to the invariant-mass distribution for each p_T interval of the analyses, varying the fit range, the functional form of the background fit function, the bin size of the invariant mass spectrum, and the width of the Gaussian function used to model the signal peaks. The latter was varied within the uncertainty of the value obtained from the fits to the prompt candidate enhanced data sample. The systematic uncertainty was defined as the root mean square of the distribution of the signal yields obtained from the described variations and ranged from 2 to 15% depending on the hadron species and the p_T interval.

The systematic uncertainty on the value of $f_{\text{non-prompt}}^{\text{raw}}$ obtained with the data-driven approach was estimated by varying the number of BDT selections employed in the data-driven method as described in Section 3.2. A systematic uncertainty ranging from 1 to 15% was assigned.

The systematic effect due to the dependence of the efficiencies on the generated p_T distribution of heavy-flavour hadrons was estimated by evaluating the production cross section after weighting the p_T shape of the PYTHIA 8 generator to match the central one predicted by FONLL calculations, as well as the upper- and lower-edge of the predictions which account for the uncertainties due to the choice of the heavy-quark masses, factorisation and renormalisation scales, and the uncertainties on the CTEQ6.6 PDFs [82]. The weights were applied to the p_T distributions of prompt charm hadrons and of the beauty hadron parent in the case of non-prompt charm hadrons. The assigned systematic uncertainty, considering the root

mean square of the production cross section distributions obtained for minimal and maximal FONLL predictions with respect to the central (default) ones, reached up to 7%.

The systematic uncertainty on the selection efficiency originates from imperfections in the description of the kinematic and topological variables of the candidates and of the detector resolutions and alignments in the simulation. It was estimated by comparing the production cross sections obtained by repeating the analysis with different selections on the BDT outputs, resulting in a significant modification of the efficiency values. The assigned systematic uncertainty ranged from 3 to 8%.

The systematic uncertainties on the track reconstruction efficiency were estimated by considering the uncertainty due to track quality selections and the uncertainty due to the TPC–ITS track matching efficiency as discussed in [21, 64]. It ranged from 2 to 6%, depending on the candidate species and p_T interval.

5 Results

5.1 Production cross sections

The p_T -differential production cross sections of non-prompt D^0 mesons, D^+ mesons, and Λ_c^+ baryons in p–Pb collisions at $\sqrt{s_{NN}} = 5.02$ TeV, measured in the rapidity interval $-0.96 < y_{cms} < 0.04$, are shown in Fig. 4 in comparison to those measured for prompt hadrons at the same center-of-mass energy [21, 64]. The measurement of prompt D^+ is the one reported in [64], scaled for the BR = $(8.98 \pm 0.28)\%$ of the $D^+ \rightarrow \pi^+ K^- \pi^+$ decay reported in [83]. The non-prompt Λ_c^+ -baryon production cross section was obtained by computing a weighted average of the production cross sections measured for the two decay channels, $\Lambda_c^+ \rightarrow p K^- \pi^+$ and $\Lambda_c^+ \rightarrow p K_S^0$, using the inverse of the quadratic sum of the relative statistical and uncorrelated systematic uncertainties as weights. The systematic uncertainties related to the tracking, luminosity, and generated p_T spectrum in the MC simulations are treated as correlated between the two decay channels; the uncertainty of the branching ratios is partially correlated as described in [75], while all the other sources of systematic uncertainties are considered fully uncorrelated.

The production cross section integrated in p_T in the visible p_T interval of the analyses and for the results extrapolated down to $p_T = 0$ are reported in Tables 2 and 3, respectively. All the systematic uncertainties were propagated as fully correlated among the measured p_T intervals, except for the one associated with the raw-yield extraction. The visible production cross sections were extrapolated down to $p_T = 0$ for non-prompt D^0 and D^+ mesons using FONLL predictions for beauty-hadron production in pp collisions and the PYTHIA 8 generator, employed to describe the decay kinematics of beauty hadrons (h_b) into charm mesons. These predictions were found to be compatible with the measurements performed in pp collisions, as shown in [36]. In order to take into account the different system sizes with respect to pp collisions, the predictions were scaled by A_{Pb} , assuming a flat B-meson R_{pPb} at unity over the whole p_T range at midrapidity, according to LHCb data [35]. The systematic uncertainties on the extrapolation factor were estimated by considering: (i) the FONLL uncertainties, (ii) the beauty fragmentation fractions $f(b \rightarrow h_b)$, (iii) the branching ratios of the $h_b \rightarrow D + X$ decays, and (iv) the variation of the p_T spectrum shape using EvtGen package for the description of the beauty-hadron decays [84]. Contribution (ii) was estimated by considering an alternative set of beauty fragmentation fractions measured in $p\bar{p}$ collisions [1] while the default one is from e^+e^- collisions. For (iii), the branching ratios implemented in PYTHIA 8 were reweighted to reproduce the measured values reported in [75]. It is not possible to extrapolate the non-prompt Λ_c^+ production cross section down to $p_T = 0$ given the absence of model calculations in p–Pb collisions for beauty baryons.

5.2 Nuclear modification factors

The nuclear modification factor R_{pPb} is computed as

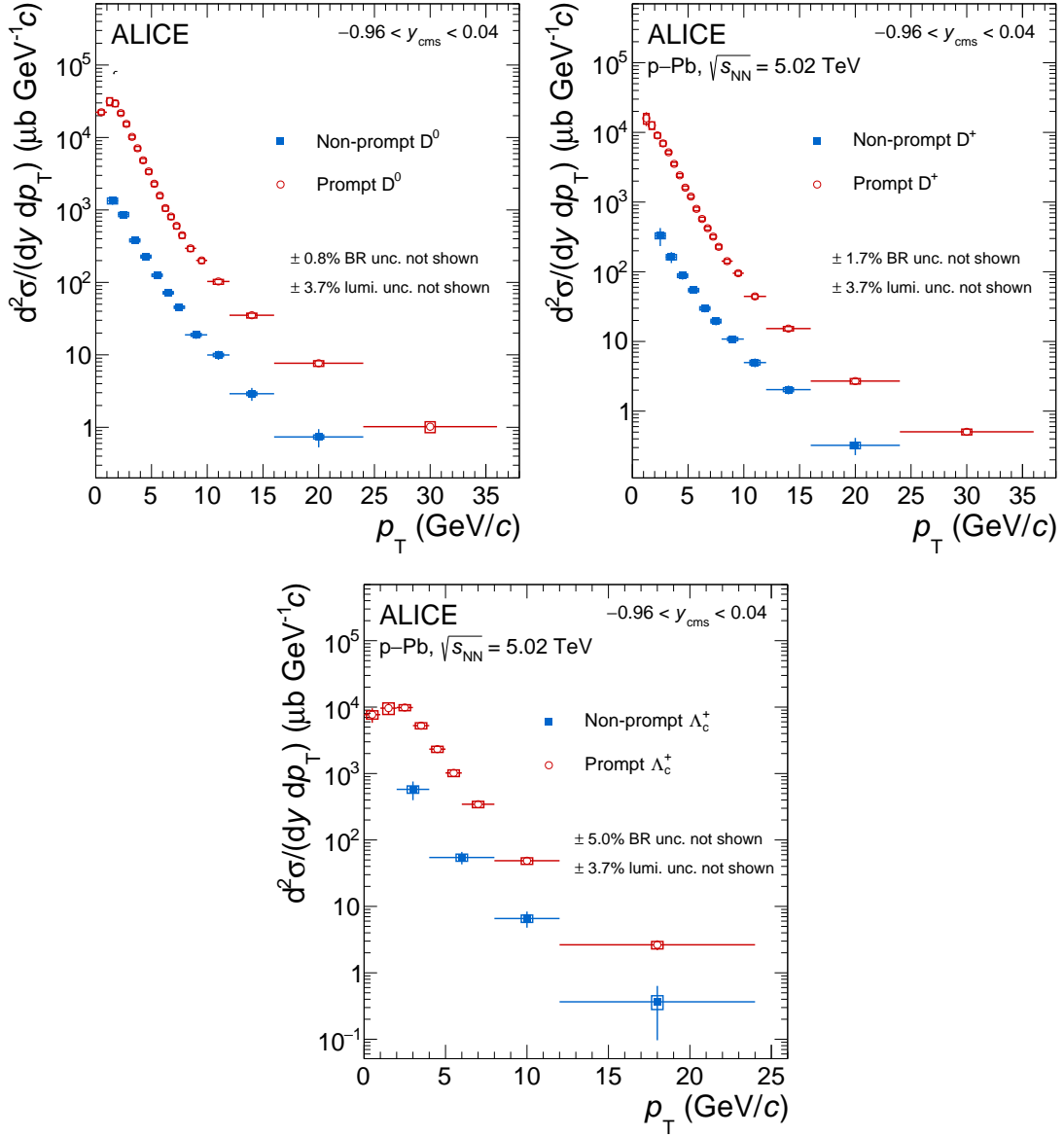


Figure 4: p_T -differential production cross sections of non-prompt D^0 , D^+ , and Λ_c^+ in p–Pb collisions at $\sqrt{s_{NN}} = 5.02$ TeV, in comparison with the corresponding production cross section of prompt hadrons from [21, 64]. The measurement of prompt D^+ mesons is the one reported in [64], with decay BR discussed in the text. The vertical bars and empty boxes represent the statistical and systematic uncertainties (without branching ratio and luminosity contributions), respectively.

$$R_{pPb} = \frac{1}{A_{Pb}} \frac{d^2\sigma_{pPb}/dp_T dy}{d^2\sigma_{pp}/dp_T dy}, \quad (3)$$

where $d^2\sigma_{pPb}/dp_T dy$ represents the p_T -differential production cross section within $-0.96 < y_{cms} < 0.04$ in p–Pb collisions at $\sqrt{s_{NN}} = 5.02$ TeV. In the analysis of the non-prompt D mesons, $d^2\sigma_{pp}/dp_T dy$ corresponds to the production cross section in pp collisions at the same center-of-mass energy at midrapidity ($|y_{lab}| < 0.5$), taken from [2]. In the case of the non-prompt Λ_c^+ analysis, the pp reference was computed adopting the non-prompt Λ_c^+ $d^2\sigma_{pp}/dp_T dy$ measured in pp collisions at $\sqrt{s} = 13$ TeV at midrapidity ($|y| < 0.5$) [36], scaled to account for the different collision energy. The scaling factor was computed as the ratio of the B production cross section from FONLL at $\sqrt{s} = 13$ and 5.02 TeV. This is justified given:

Table 2: Production cross sections in the measured p_T range for non-prompt charm hadrons in p–Pb collisions at $\sqrt{s_{NN}} = 5.02$ TeV.

Hadron	Kinematic range (GeV/c)	$d\sigma_{pPb}^{\text{visible}}/dy _{ y_{\text{lab}} <0.5}$ (μb)
D^0	$1 < p_T < 24$	3128 ± 183 (stat.) ± 187 (syst.) ± 116 (lumi.) ± 24 (BR)
D^+	$2 < p_T < 24$	726 ± 101 (stat.) ± 42 (syst.) ± 27 (lumi.) ± 12 (BR)
Λ_c^+	$2 < p_T < 24$	1404 ± 364 (stat.) ± 171 (syst.) ± 52 (lumi.) ± 70 (BR)

Table 3: Production cross sections in the range $p_T > 0$ for non-prompt charm hadrons in p–Pb collisions at $\sqrt{s_{NN}} = 5.02$ TeV.

Hadron	Extr. factor to $p_T > 0$	$d\sigma_{pPb}/dy _{ y_{\text{lab}} <0.5}$ (μb)
D^0	$1.275^{+0.014}_{-0.048}$	3989 ± 234 (stat.) ± 282 (syst.) ± 148 (lumi.) ± 30 (BR) $^{+200}_{-307}$ (extr.)
D^+	$2.21^{+0.05}_{-0.19}$	1604 ± 222 (stat.) ± 111 (syst.) ± 59 (lumi.) ± 27 (BR) $^{+36}_{-140}$ (extr.)

(i) the compatible p_T -dependence of the 13-to-5.02 TeV ratio of mesons and baryons in the charm sector at midrapidity [6], (ii) the agreement with the FONLL calculations of charm mesons at midrapidity and beauty meson at forward rapidity [85, 86], and (iii) the assumption that the beauty baryons have a similar scaling as the beauty mesons, as observed in the charm sector [36]. A similar behavior is found in the beauty sector [87], though with much larger uncertainties. The shift in rapidity between pp and p–Pb collisions was corrected by using FONLL predictions for the B meson production cross sections in the two rapidity intervals, and applying the estimated correction to the non-prompt D^0 , D^+ , and Λ_c^+ measurements. The corresponding correction ranges from 0.9 to 2.3%, increasing at higher p_T [64]. The systematic uncertainties of the p–Pb and pp measurements were treated as uncorrelated within the same p_T interval and were propagated quadratically, with the exception of the BR which cancels out in the ratio.

The non-prompt D^0 and D^+ R_{pPb} are compatible over the full p_T range within the current uncertainties. In order to have a more precise measurement, the average of their R_{pPb} was computed, using the inverse of the quadratic sum of the statistical and uncorrelated systematic uncertainties as weights. The systematic uncertainty of the average was computed by propagating the uncertainties through the weighted average while assuming the contributions from tracking efficiency and normalisation to be fully correlated.

The left panel of Fig. 5 shows the average R_{pPb} of non-prompt D^0 and D^+ mesons, and the average R_{pPb} of prompt D^0 , D^+ , and D^{*+} mesons [64]. The R_{pPb} of prompt and non-prompt charm mesons are compatible with each other and with unity over the entire p_T interval of the measurements within the statistical and systematic uncertainties. The comparison between the R_{pPb} of prompt [21] and non-prompt Λ_c^+ baryons is shown in the right panel of Fig. 5. The prompt Λ_c^+ -baryon R_{pPb} shows deviation from unity, highlighting modifications of the p_T spectrum in p–Pb collisions with respect to pp collisions, due to effects beyond nPDFs that may relate to the hadronisation process or to the presence of an expanding medium [26]. The non-prompt Λ_c^+ -baryon R_{pPb} is compatible both with unity and with the prompt Λ_c^+ -baryon measurements. Given its large uncertainties, it is not possible to conclude about a possible trend versus p_T .

The p_T -integrated R_{pPb} values for non-prompt D^0 and D^+ mesons in $-0.96 < y_{\text{cms}} < 0.04$ were calculated from the extrapolated p_T -integrated production cross sections reported above and the non-prompt D^0 - and D^+ -meson production cross sections measured in pp collisions at $\sqrt{s} = 5.02$ TeV [2]. The resulting R_{pPb} values of non-prompt D^0 and D^+ mesons in p–Pb collisions are:

$$R_{pPb}^{\text{non-prompt } D^0}(p_T > 0, -0.96 < y_{\text{cms}} < 0.04) = 1.04 \pm 0.11(\text{stat.}) \pm 0.12(\text{syst.})^{+0.06}_{-0.11}(\text{extr.}),$$

$$R_{pPb}^{\text{non-prompt } D^+}(p_T > 0, -0.96 < y_{\text{cms}} < 0.04) = 0.86 \pm 0.19(\text{stat.}) \pm 0.11(\text{syst.})^{+0.03}_{-0.11}(\text{extr.}).$$

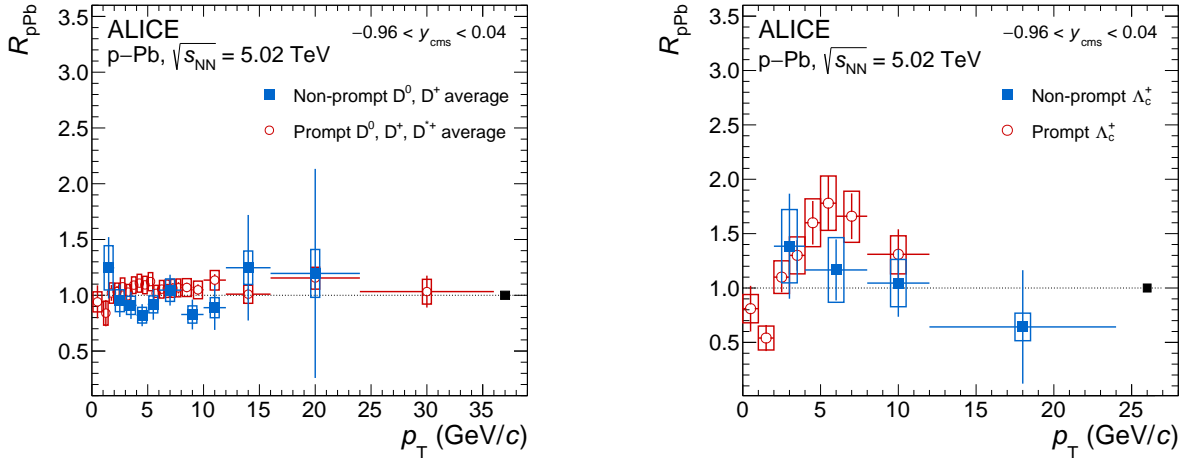


Figure 5: Left panel: average p_T -differential R_{pPb} of prompt D^0 , D^+ , and D^* [64], and non-prompt D^0 and D^+ mesons. Right panel: p_T -differential R_{pPb} of prompt [21] and non-prompt Λ_c^+ baryons. The vertical bars and empty boxes represent the statistical and systematic uncertainties, respectively. The black-filled box at $R_{pPb} = 1$ represents the normalisation systematic uncertainty.

The p_T -integrated R_{pPb} values of non-prompt D mesons are compatible with unity within uncertainties, which is consistent with a not significant modification of production cross section in p–Pb collisions compared to pp collisions, as observed in the charm sector [36].

The left panel of Fig. 6 shows the p_T -integrated R_{pPb} measured at midrapidity for non-prompt D^0 , D^+ , and J/ψ mesons by the ALICE Collaboration [88] compared to the ones of non-prompt J/ψ and B^+ mesons measured at forward ($1.5 < y_{cms} < 4.0$, $2.5 < y_{cms} < 3.5$) and backward ($-5.0 < y_{cms} < -2.5$, $-3.5 < y_{cms} < -2.5$) rapidity by the LHCb Collaboration [35, 89]. The measurements of non-prompt D, J/ψ , and B mesons in p–Pb collisions at forward, backward, and midrapidity exploring different Bjorken- x regions, are sensitive to different levels of shadowing and saturation regimes. The experimental results of p_T -integrated R_{pPb} are compared with model calculations of the B^+ meson in p–Pb/Pb–p collisions at $\sqrt{s_{NN}} = 8.16$ TeV using the HELAC-onia generator [90–92] with three different sets of nPDFs, i.e. EPPS16 [54], nCTEQ15 [93], and EPPS16* [58]. In the calculations with EPPS16 and nCTEQ15, the model parameters are tuned to reproduce J/ψ and $\psi(2S)$ cross section measurements in pp collisions at the LHC [94, 95]. A weighting based on several heavy-flavour measurements was applied on the nPDF set EPPS16 [54], to obtain the nPDF set EPPS16*, as explained in [58]. The uncertainties in the theoretical predictions arise from those of the corresponding nPDF parameterisations. The measurements agree with the model calculations within the uncertainties.

The right panel of Fig. 6 shows the p_T -integrated nuclear modification factors of prompt [64] and non-prompt D^0 mesons measured in p–Pb collisions compared with those measured in central (0-10%) [96] and semicentral (30-50%) [97] Pb–Pb collisions. These measurements provide an additional tool to investigate the modification of heavy-flavour production from pp to p–Pb and Pb–Pb collisions in the beauty sector. A p_T -integrated R_{pPb} compatible with unity is measured for both prompt and non-prompt charm mesons, suggesting the overall CNM effects in the charm and beauty sector are similar in p–Pb collisions. In Pb–Pb collisions, a hint of a different behaviour between charm and beauty is suggested, possibly due to a higher sensitivity of charm quarks to the nPDF modification (shadowing). Extending the measurement of beauty hadron production down to $p_T = 0$, both in p–Pb and Pb–Pb collisions, will be crucial to finally achieve a complete understanding of possible modification of the heavy-flavour production due to CNM effects and possible different hadronisation mechanisms across collision systems.

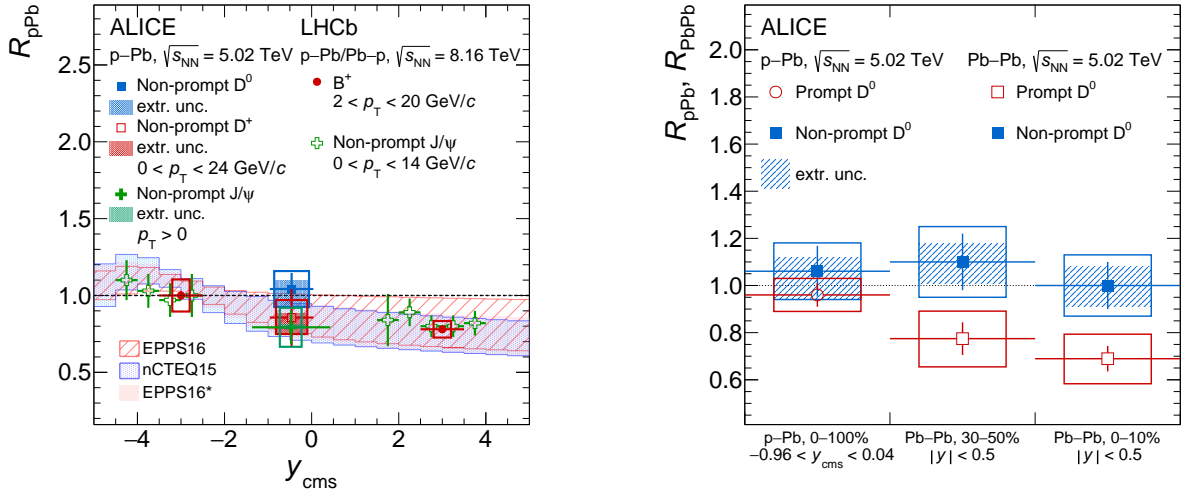


Figure 6: Left panel: Nuclear modification factors of non-prompt D^0 and D^+ mesons measured in p–Pb collisions at $\sqrt{s_{NN}} = 5.02$ TeV compared with the measurement of non-prompt J/ψ at midrapidity [88], and the measurements of non-prompt J/ψ and B^+ mesons at forward and backward rapidity [35, 89]. The results are also compared with B-meson R_{pPb} calculations using different nPDF sets [54, 58, 93]. Right panel: p_T -integrated nuclear modification factor of prompt and non-prompt D^0 mesons measured in p–Pb and Pb–Pb collisions at $\sqrt{s_{NN}} = 5.02$ TeV [64, 96, 97]. Statistical (bars) and systematic (boxes) uncertainties are shown. Extrapolation uncertainties of non-prompt D^0 mesons in p–Pb and Pb–Pb collisions are shown separately as shaded bands.

5.3 Production cross section ratios

To probe hadronisation in p–Pb collisions and its possible modification with respect to smaller collision systems, ratios of non-prompt D^+ over non-prompt D^0 , and non-prompt Λ_c^+ over non-prompt D^0 p_T -integrated production cross sections were computed. The systematic uncertainties were propagated to the ratios as uncorrelated except for the ones related to tracking efficiency and normalisation, which were treated as fully correlated. The ratios are reported in Tables 4 and 5, respectively.

The non-prompt D^+/D^0 p_T -integrated yield ratios are reported in Table 4, together with the values measured in pp collisions [2] at $\sqrt{s} = 5.02$ TeV and with the one measured in e^+e^- collisions at LEP [1], where the error includes the statistical uncertainties, systematic uncertainties and the uncertainties from the relevant branching fractions. The results are compatible within experimental uncertainties, and no dependence on the collision system or energy is observed.

Table 4: Production cross section ratios of non-prompt D^+ over D^0 for the measured p_T ranges at midrapidity ($|y_{lab}| < 0.5$) in pp collisions at $\sqrt{s} = 5.02$ TeV [2], p–Pb collisions at $\sqrt{s_{NN}} = 5.02$ TeV, and in e^+e^- collisions at $\sqrt{s} = 209$ GeV at LEP [1].

System	Kinematic range (GeV/c)	Non-prompt D^+/D^0
pp at $\sqrt{s} = 5.02$ TeV [2]	$2 < p_T < 24$	0.487 ± 0.090 (stat.) ± 0.055 (syst.) ± 0.009 (BR)
p–Pb at $\sqrt{s_{NN}} = 5.02$ TeV	$2 < p_T < 24$	0.402 ± 0.060 (stat.) ± 0.034 (syst.) ± 0.011 (BR)
e^+e^- at $\sqrt{s} = 209$ GeV LEP average [1]	–	0.380 ± 0.025

A possible p_T dependence was investigated by computing the p_T -differential ratios. The ratios of the p_T -differential production cross sections for prompt and non-prompt D^+/D^0 are shown in the left panel of Fig. 7. The non-prompt D^+/D^0 ratio is independent of p_T in the measured p_T range within the current experimental precision and is compatible with the prompt D^+/D^0 ratio pointing to a similar

hadronisation of charm and beauty quarks to open heavy-flavour mesons at midrapidity. This result is in line with what was observed in the same rapidity interval in pp and Pb–Pb collisions at different collision energies [2, 96]. In the right panel of Fig. 7, the non-prompt D^+/D^0 ratio measured in p–Pb collisions is compared with the non-prompt D^+/D^0 ratio measured in pp collisions at the same collision energy. The two measurements are compatible over the full p_T range of the measurements within the uncertainties, pointing to no significant modification of beauty quarks to mesons within uncertainties.

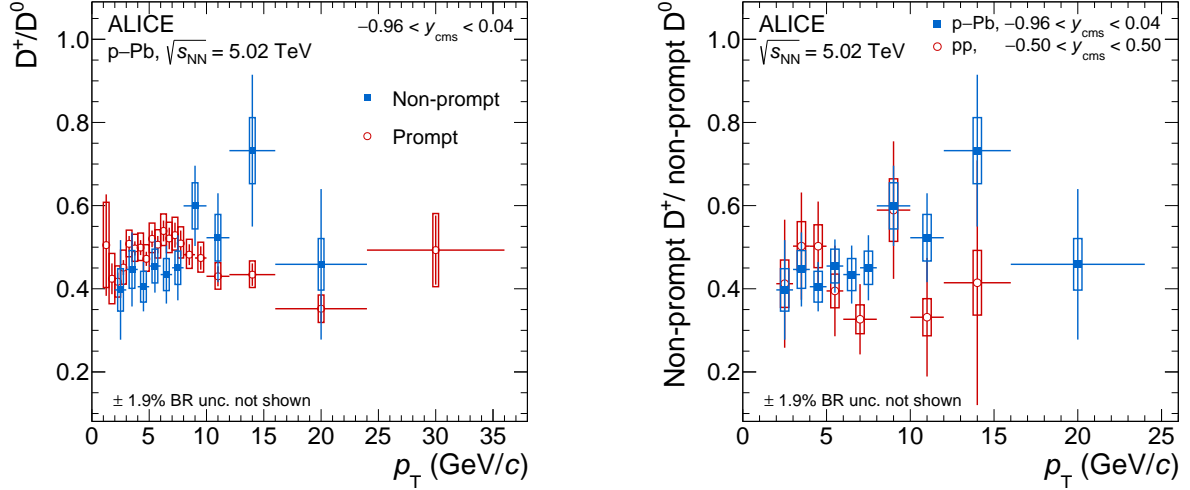


Figure 7: Left panel: prompt (red) [64] and non-prompt (blue) D^+/D^0 yield ratio as a function of p_T . Right panel: non-prompt D^+/D^0 yield ratios as a function of p_T measured by ALICE Collaboration in pp (red) [2] and p–Pb (blue) collisions at the same collision energy. The vertical bars and empty boxes represent the statistical and systematic uncertainties (without the branching ratio contribution), respectively.

The ratio between the p_T -integrated production cross sections of non-prompt Λ_c^+ and D^0 hadrons is reported in Table 5, together with the one measured in pp collisions at $\sqrt{s} = 13$ TeV ($|y| < 0.5$) [36] and the one measured at LEP [1]. Despite the different collision energies, an agreement within the experimental uncertainties is observed between the measurements performed in pp and p–Pb collisions. On the other hand, a significant difference is observed when comparing them with the e^+e^- measurement obtained at LEP exhibiting a significant enhancement in the measured p_T range, with respect to the meson production at midrapidity in the beauty sector, as observed in the charm sector [36].

Table 5: Cross sections ratios of non-prompt Λ_c^+ and D^0 for the measured p_T ranges at midrapidity ($|y_{\text{lab}}| < 0.5$) in pp collisions at $\sqrt{s} = 13$ TeV [36], p–Pb collisions at $\sqrt{s_{\text{NN}}} = 5.02$ TeV, and in e^+e^- collisions at $\sqrt{s} = 209$ GeV at LEP [1].

System	Kinematic range (GeV/c)	Non-prompt Λ_c^+/D^0
pp at $\sqrt{s} = 13$ TeV [36]	$2 < p_T < 24$	0.55 ± 0.07 (stat.) ± 0.06 (syst.)
p–Pb at $\sqrt{s_{\text{NN}}} = 5.02$ TeV	$2 < p_T < 24$	0.78 ± 0.21 (stat.) ± 0.22 (syst.)
e^+e^- at $\sqrt{s} = 209$ GeV, LEP average [1]	–	0.124 ± 0.016

In order to gain further information about modification of hadronisation mechanisms in the beauty sector, the ratio of the p_T -differential production cross sections of non-prompt Λ_c^+ and D^0 hadrons measured in p–Pb collisions at $\sqrt{s_{\text{NN}}} = 5.02$ TeV is computed and shown in the top-left panel of Fig. 8. It is compared to the analogous ratio measured in pp collisions at $\sqrt{s} = 13$ TeV [36] and with the Λ_b^0/B^0 ratio measured by the LHCb Collaboration at forward rapidity ($2 < y_{\text{lab}} < 4.5$) in pp collisions at $\sqrt{s} = 13$ TeV [24]. The baryon-to-meson ratio shows a decreasing trend with increasing p_T in both pp and p–Pb collisions. The baryon enhancement suggested at low p_T is qualitatively similar to what was measured in pp collisions, where it was explained by different modelling of hadronisation mechanisms beyond pure

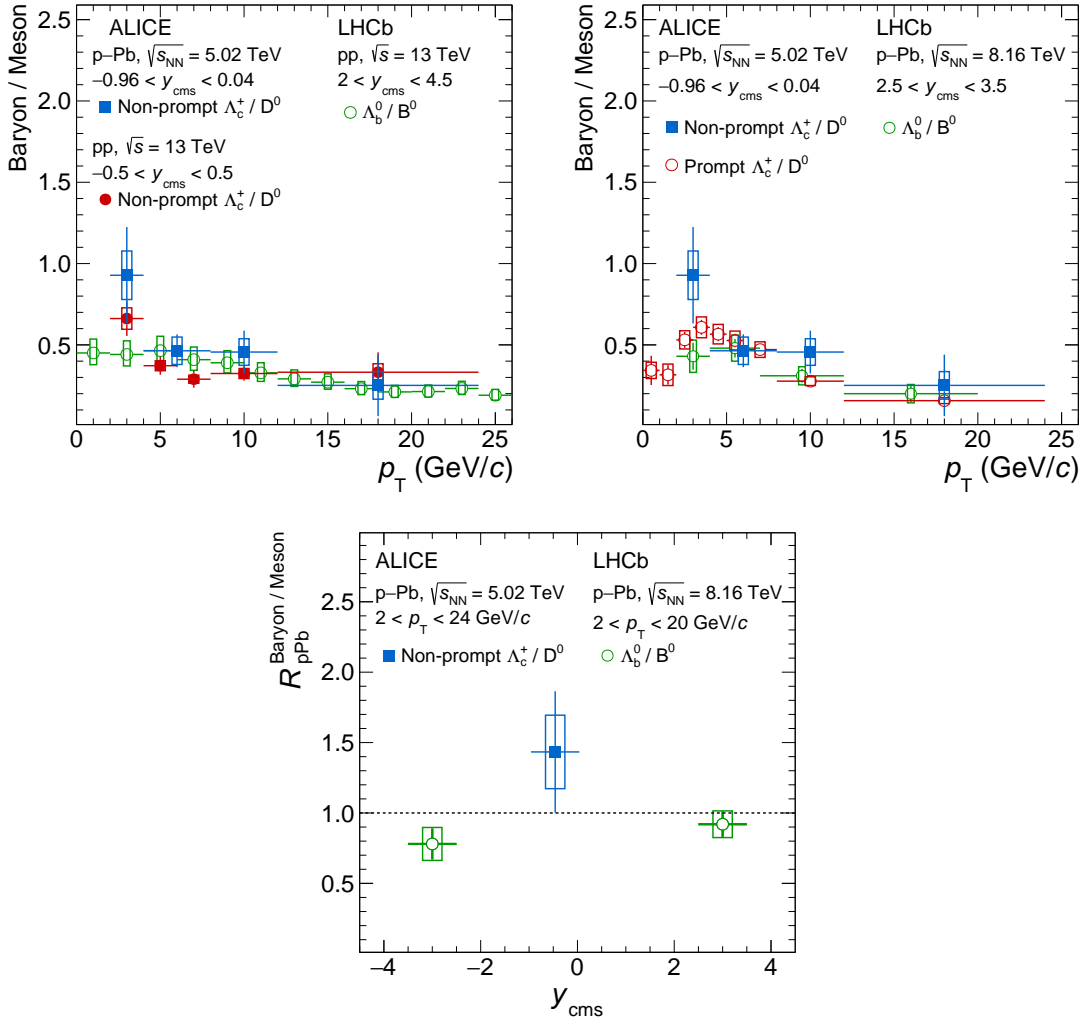


Figure 8: Top-left panel: non-prompt Λ_c^+ / D^0 yield ratios as a function of p_T measured by ALICE in pp (red) [36] and p–Pb (blue) collisions compared with the Λ_b^0 / B^0 ratio (green) [24] measured by the LHCb Collaboration at forward rapidity ($2 < y_{lab} < 4.5$) in pp collisions. Top-right panel: prompt (red) [21] and non-prompt (blue) Λ_c^+ / D^0 yield ratios as a function of p_T measured by ALICE in $-0.96 < y_{cms} < 0.04$ together with the Λ_b^0 / B^0 yield ratio (green) [35] measured by LHCb in $2.5 < y_{cms} < 3.5$. Bottom panel: ratios of the nuclear modification factor of non-prompt Λ_c^+ and non-prompt D^0 at midrapidity (blue), and the Λ_b^0 and B^0 at forward and backward rapidity measured by LHCb (red) [35].

in-vacuum fragmentation. Notable among these are the coalescence or recombination of charm quarks with quarks from a thermal medium [40, 42, 43], the statistical hadronisation that takes into account undiscovered higher charm resonant states [45, 46], and the string formation beyond the leading colour approximation [47, 48]. The lack of similar models for the beauty hadrons in p–Pb collisions, that could also account for the presence of the Pb nucleons in the collisions, prevents any conclusion about the origin of this modification in p–Pb collisions. Neglecting a possible dependence on the collision energy, which is not observed in the charm sector [6], the measurement in p–Pb collisions hints at a higher non-prompt Λ_c^+ / D^0 yield ratio in $2 < p_T < 12$ GeV/c with respect to the pp one, similarly to what is more precisely measured for the prompt Λ_c^+ / D^0 [21] and Ξ_c^0 / D^0 ratios [98] and for the Λ_b^0 / B^0 ratio ($-3.5 < y_{lab} < -2.5$ and $2.5 < y_{lab} < 3.5$) [35]. This difference suggests a possible hardening of the beauty baryon p_T spectra, consistent with a radial flow scenario, where the shift to higher p_T depends on the particle mass. Similar spectrum modifications in p–Pb collisions were also observed in the strangeness sector by the ALICE and CMS Collaborations [60, 99], and were found to be in line with the effect of radial flow predicted by

hydrodynamic models such as EPOS LHC [100]. Future precise measurements down to $p_T = 0$ will be crucial to assess potential differences on the beauty baryon yields and collective motion in pp and p–Pb collisions.

As shown in the top-right panel of Fig. 8, the non-prompt baryon-to-meson ratio is compatible with the prompt Λ_c^+/D^0 [21] within the uncertainties in the measured p_T range in p–Pb collisions at $\sqrt{s_{NN}} = 5.02$ TeV. The results are also compared with the Λ_b^0/B^0 yield ratio measured by the LHCb Collaboration at $2.5 < y_{cms} < 3.5$ [35] in p–Pb collisions at $\sqrt{s_{NN}} = 8.16$ TeV. The LHCb measurement is compatible with both the prompt and non-prompt Λ_c^+/D^0 ratios, despite the difference in energy, rapidity, and the slight difference in p_T coverage between the ALICE and LHCb measurements. This suggests that the hadronisation modifications for beauty quarks may mirror those for charm quarks [37]. The Λ_b^0/B^0 ratio from the LHCb Collaboration is lower than the non-prompt Λ_c^+/D^0 ratio in the low- p_T interval when compared to both collision systems. However, the large experimental uncertainties over the full p_T ranges prevent from drawing strong conclusions.

Assuming that the modifications of hadronisation mechanisms of heavy quarks are similar in pp and p–Pb collisions, one would expect the double ratio of non-prompt Λ_c^+ (Λ_b^0) over D^0 (B^0) production in p–Pb to pp collisions (non-prompt $R_{pPb}^{\Lambda_c^+/D^0}$ or $R_{pPb}^{\Lambda_b^0/B^0}$) to be consistent with unity. This quantity corresponds to the ratio of nuclear modification factors of baryons over mesons. The bottom panel of Fig. 8 shows the p_T -integrated ($p_T > 2$ GeV/c) R_{pPb} of non-prompt Λ_c^+ baryons divided by that of non-prompt D^0 mesons, compared with the same ratio for Λ_b^0 baryons and B^0 mesons measured by the LHCb Collaboration [35] as a function of y_{cms} . The result in $-0.96 < y_{cms} < 0.04$ is consistent with unity within the uncertainties. However, more precise measurements exploiting larger collected data samples, are required to conclude on a possible rapidity dependence of beauty-baryon hadronisation.

6 Summary

The first measurements of non-prompt D^{0-} , D^{+-} , and Λ_c^+ -hadron production at midrapidity in p–Pb collisions are reported. Extrapolating the visible non-prompt D meson production cross sections down to $p_T = 0$, the p_T -integrated R_{pPb} of D mesons is computed. Within the uncertainties, the p_T -integrated R_{pPb} of non-prompt D mesons is consistent with unity. Similarly, the p_T -integrated R_{pPb} of non-prompt D^0 is compatible with prompt D^0 . The p_T -differential R_{pPb} of non-prompt D mesons and Λ_c^+ is compatible with unity and the measurements in the charm sector, in the measured p_T range, within uncertainties. However, due to the current experimental uncertainties, it remains challenging to clearly differentiate between a flat trend compatible with unity, and the trend observed for prompt Λ_c^+ in p–Pb collisions as a function of p_T . The prompt and non-prompt yield ratios are compatible within current experimental uncertainties for both D^+/D^0 and Λ_c^+/D^0 . The p_T -differential non-prompt Λ_c^+/D^0 in p–Pb collisions is compatible with the non-prompt Λ_c^+/D^0 ratio and Λ_b^0/B^0 ratio measured in pp collisions. The p_T -integrated non-prompt $R_{pPb}^{\Lambda_c^+/D^0}$ was measured at midrapidity and is compatible with the p_T -integrated $R_{pPb}^{\Lambda_b^0/B^0}$ measured by the LHCb Collaboration. The results indicate no significant CNM effects in the beauty sector within uncertainties. These novel measurements in p–Pb collisions provide important insights, enriching the understanding of nPDF models and the modification of beauty quark hadronisation mechanisms. In addition, these measurements represent an important input for constraining theoretical models for heavy-flavour hadron production in p–Pb collisions, which are still lacking at the moment. With the major upgrade of the ALICE detector for Run 3, larger data samples, and foreseen upgrades for Run 4, ALICE will significantly advance this field in the near future.

Acknowledgements

The ALICE Collaboration would like to thank all its engineers and technicians for their invaluable contributions to the construction of the experiment and the CERN accelerator teams for the outstanding performance of the LHC complex. The ALICE Collaboration gratefully acknowledges the resources and support provided by all Grid centres and the Worldwide LHC Computing Grid (WLCG) collaboration. The ALICE Collaboration acknowledges the following funding agencies for their support in building and running the ALICE detector: A. I. Alikhanyan National Science Laboratory (Yerevan Physics Institute) Foundation (ANSL), State Committee of Science and World Federation of Scientists (WFS), Armenia; Austrian Academy of Sciences, Austrian Science Fund (FWF): [M 2467-N36] and Nationalstiftung für Forschung, Technologie und Entwicklung, Austria; Ministry of Communications and High Technologies, National Nuclear Research Center, Azerbaijan; Conselho Nacional de Desenvolvimento Científico e Tecnológico (CNPq), Financiadora de Estudos e Projetos (Finep), Fundação de Amparo à Pesquisa do Estado de São Paulo (FAPESP) and Universidade Federal do Rio Grande do Sul (UFRGS), Brazil; Bulgarian Ministry of Education and Science, within the National Roadmap for Research Infrastructures 2020-2027 (object CERN), Bulgaria; Ministry of Education of China (MOEC), Ministry of Science & Technology of China (MSTC) and National Natural Science Foundation of China (NSFC), China; Ministry of Science and Education and Croatian Science Foundation, Croatia; Centro de Aplicaciones Tecnológicas y Desarrollo Nuclear (CEADEN), Cubaenergía, Cuba; Ministry of Education, Youth and Sports of the Czech Republic, Czech Republic; The Danish Council for Independent Research | Natural Sciences, the VILLUM FONDEN and Danish National Research Foundation (DNRF), Denmark; Helsinki Institute of Physics (HIP), Finland; Commissariat à l’Energie Atomique (CEA) and Institut National de Physique Nucléaire et de Physique des Particules (IN2P3) and Centre National de la Recherche Scientifique (CNRS), France; Bundesministerium für Bildung und Forschung (BMBF) and GSI Helmholtzzentrum für Schwerionenforschung GmbH, Germany; General Secretariat for Research and Technology, Ministry of Education, Research and Religions, Greece; National Research, Development and Innovation Office, Hungary; Department of Atomic Energy Government of India (DAE), Department of Science and Technology, Government of India (DST), University Grants Commission, Government of India (UGC) and Council of Scientific and Industrial Research (CSIR), India; National Research and Innovation Agency - BRIN, Indonesia; Istituto Nazionale di Fisica Nucleare (INFN), Italy; Japanese Ministry of Education, Culture, Sports, Science and Technology (MEXT) and Japan Society for the Promotion of Science (JSPS) KAKENHI, Japan; Consejo Nacional de Ciencia (CONACYT) y Tecnología, through Fondo de Cooperación Internacional en Ciencia y Tecnología (FONCICYT) and Dirección General de Asuntos del Personal Académico (DGAPA), Mexico; Nederlandse Organisatie voor Wetenschappelijk Onderzoek (NWO), Netherlands; The Research Council of Norway, Norway; Pontificia Universidad Católica del Perú, Peru; Ministry of Science and Higher Education, National Science Centre and WUT ID-UB, Poland; Korea Institute of Science and Technology Information and National Research Foundation of Korea (NRF), Republic of Korea; Ministry of Education and Scientific Research, Institute of Atomic Physics, Ministry of Research and Innovation and Institute of Atomic Physics and Universitatea Nationala de Stiinta si Tehnologie Politehnica Bucuresti, Romania; Ministry of Education, Science, Research and Sport of the Slovak Republic, Slovakia; National Research Foundation of South Africa, South Africa; Swedish Research Council (VR) and Knut & Alice Wallenberg Foundation (KAW), Sweden; European Organization for Nuclear Research, Switzerland; Suranaree University of Technology (SUT), National Science and Technology Development Agency (NSTDA) and National Science, Research and Innovation Fund (NSRF via PMU-B B05F650021), Thailand; Turkish Energy, Nuclear and Mineral Research Agency (TENMAK), Turkey; National Academy of Sciences of Ukraine, Ukraine; Science and Technology Facilities Council (STFC), United Kingdom; National Science Foundation of the United States of America (NSF) and United States Department of Energy, Office of Nuclear Physics (DOE NP), United States of America. In addition, individual groups or members have received support from: Czech Science Foundation (grant no. 23-07499S), Czech Republic; European Research

Council (grant no. 950692), European Union; ICSC - Centro Nazionale di Ricerca in High Performance Computing, Big Data and Quantum Computing, European Union - NextGenerationEU; Academy of Finland (Center of Excellence in Quark Matter) (grant nos. 346327, 346328), Finland.

References

- [1] L. Gladilin, “Fragmentation fractions of c and b quarks into charmed hadrons at LEP”, *Eur. Phys. J. C* **75** (2015) 19, arXiv:1404.3888 [hep-ex].
- [2] **ALICE** Collaboration, S. Acharya *et al.*, “Measurement of beauty and charm production in pp collisions at $\sqrt{s} = 5.02$ TeV via non-prompt and prompt D mesons”, *JHEP* **05** (2021) 220, arXiv:2102.13601 [nucl-ex].
- [3] **ALICE** Collaboration, S. Acharya *et al.*, “Measurement of D-meson production at mid-rapidity in pp collisions at $\sqrt{s} = 7$ TeV”, *Eur. Phys. J. C* **77** (2017) 550, arXiv:1702.00766 [hep-ex].
- [4] **LHCb** Collaboration, R. Aaij *et al.*, “Measurements of prompt charm production cross-sections in pp collisions at $\sqrt{s} = 5$ TeV”, *JHEP* **06** (2017) 147, arXiv:1610.02230 [hep-ex].
- [5] **CMS** Collaboration, A. Tumasyan *et al.*, “Measurement of prompt open-charm production cross sections in proton–proton collisions at $\sqrt{s} = 13$ TeV”, *JHEP* **11** (2021) 225, arXiv:2107.01476 [hep-ex].
- [6] **ALICE** Collaboration, S. Acharya *et al.*, “Charm production and fragmentation fractions at midrapidity in pp collisions at $\sqrt{s} = 13$ TeV”, *JHEP* **12** (2023) 086, arXiv:2308.04877 [hep-ex].
- [7] **ALICE** Collaboration, J. Adam *et al.*, “D-meson production in p–Pb collisions at $\sqrt{s_{NN}} = 5.02$ TeV and in pp collisions at $\sqrt{s} = 7$ TeV”, *Phys. Rev. C* **94** (2016) 054908, arXiv:1605.07569 [nucl-ex].
- [8] **CMS** Collaboration, A. Tumasyan *et al.*, “Measurement of the dependence of the hadron production fraction ratio f_s/f_u and f_d/f_u on B meson kinematic variables in proton-proton collisions at $\sqrt{s} = 13$ TeV”, *Phys. Rev. Lett.* **131** (2023) 121901, arXiv:2212.02309 [hep-ex].
- [9] **ATLAS** Collaboration, G. Aad *et al.*, “Measurement of $D^{*\pm}$, D^\pm and D_s^\pm meson production cross sections in pp collisions at $\sqrt{s} = 7$ TeV with the ATLAS detector”, *Nucl. Phys. B* **907** (2016) 717–763, arXiv:1512.02913 [hep-ex].
- [10] **ATLAS** Collaboration, G. Aad *et al.*, “Measurement of the differential cross-section of B^+ meson production in pp collisions at $\sqrt{s} = 7$ TeV at ATLAS”, *JHEP* **10** (2013) 042, arXiv:1307.0126 [hep-ex].
- [11] **ATLAS** Collaboration, G. Aad *et al.*, “Determination of the ratio of b -quark fragmentation fractions f_s/f_d in pp collisions at $\sqrt{s} = 7$ TeV with the ATLAS detector”, *Phys. Rev. Lett.* **115** (2015) 262001, arXiv:1507.08925 [hep-ex].
- [12] **ATLAS** Collaboration, M. Aaboud *et al.*, “Measurement of the relative B_c^\pm/B^\pm production cross section with the ATLAS detector at $\sqrt{s} = 8$ TeV”, *Phys. Rev. D* **104** (2021) 012010, arXiv:1912.02672 [hep-ex].
- [13] M. Cacciari, M. Greco, and P. Nason, “The p_T spectrum in heavy flavor hadroproduction”, *JHEP* **05** (1998) 007, arXiv:hep-ph/9803400.

- [14] M. Cacciari, S. Frixione, N. Houdeau, M. L. Mangano, P. Nason, and G. Ridolfi, “Theoretical predictions for charm and bottom production at the LHC”, *JHEP* **10** (2012) 137, arXiv:1205.6344 [hep-ph].
- [15] B. A. Kniehl, G. Kramer, I. Schienbein, and H. Spiesberger, “Inclusive $D^{*\pm}$ production in p anti-p collisions with massive charm quarks”, *Phys. Rev. D* **71** (2005) 014018, arXiv:hep-ph/0410289.
- [16] B. A. Kniehl, G. Kramer, I. Schienbein, and H. Spiesberger, “Collinear subtractions in hadroproduction of heavy quarks”, *Eur. Phys. J. C* **41** (2005) 199–212, arXiv:hep-ph/0502194.
- [17] B. A. Kniehl, G. Kramer, I. Schienbein, and H. Spiesberger, “Inclusive Charmed-Meson Production at the CERN LHC”, *Eur. Phys. J. C* **72** (2012) 2082, arXiv:1202.0439 [hep-ph].
- [18] I. Helenius and H. Paukkunen, “Revisiting the D-meson hadroproduction in general-mass variable flavour number scheme”, *JHEP* **05** (2018) 196, arXiv:1804.03557 [hep-ph].
- [19] T. Sjöstrand, S. Ask, J. R. Christiansen, R. Corke, N. Desai, P. Ilten, S. Mrenna, S. Prestel, C. O. Rasmussen, and P. Z. Skands, “An introduction to PYTHIA 8.2”, *Comput. Phys. Commun.* **191** (2015) 159–177, arXiv:1410.3012 [hep-ph].
- [20] P. Skands, S. Carrazza, and J. Rojo, “Tuning PYTHIA 8.1: the Monash 2013 Tune”, *Eur. Phys. J. C* **74** (2014) 3024, arXiv:1404.5630 [hep-ph].
- [21] ALICE Collaboration, S. Acharya *et al.*, “First measurement of Λ_c^+ production down to $p_T = 0$ in pp and p-Pb collisions at $\sqrt{s_{NN}} = 5.02$ TeV”, *Phys. Rev. C* **107** (2023) 064901, arXiv:2211.14032 [nucl-ex].
- [22] ALICE Collaboration, S. Acharya *et al.*, “Measurement of the cross sections of Ξ_c^0 and Ξ_c^+ Baryons and of the branching-fraction ratio $BR(\Xi_c^0 \rightarrow \Xi^- e^+ \nu_e)/BR(\Xi_c^0 \rightarrow \Xi^- \pi^+)$ in pp collisions at 13 TeV”, *Phys. Rev. Lett.* **127** (2021) 272001, arXiv:2105.05187 [nucl-ex].
- [23] ALICE Collaboration, S. Acharya *et al.*, “First measurement of Ω_c^0 production in pp collisions at $s=13$ TeV”, *Phys. Lett. B* **846** (2023) 137625, arXiv:2205.13993 [nucl-ex].
- [24] LHCb Collaboration, R. Aaij *et al.*, “Enhanced production of Λ_b^0 baryons in high-multiplicity pp collisions at $\sqrt{s} = 13$ TeV”, *Phys. Rev. Lett.* **132** (2024) 081901, arXiv:2310.12278 [hep-ex].
- [25] ALICE Collaboration, S. Acharya *et al.*, “ Λ_c^+ production in pp collisions at $\sqrt{s} = 7$ TeV and in p–Pb collisions at $\sqrt{s_{NN}} = 5.02$ TeV”, *JHEP* **04** (2018) 108, arXiv:1712.09581 [nucl-ex].
- [26] ALICE Collaboration, S. Acharya *et al.*, “ Λ_c^+ production in pp and in p–Pb collisions at $\sqrt{s_{NN}} = 5.02$ TeV”, *Phys. Rev. C* **104** (2021) 054905, arXiv:2011.06079 [nucl-ex].
- [27] ALICE Collaboration, S. Acharya *et al.*, “ Λ_c^+ production and baryon-to-meson ratios in pp and p–Pb collisions at $\sqrt{s_{NN}} = 5.02$ TeV at the LHC”, *Phys. Rev. Lett.* **127** (2021) 202301, arXiv:2011.06078 [nucl-ex].
- [28] CMS Collaboration, A. M. Sirunyan *et al.*, “Production of Λ_c^+ baryons in proton-proton and lead-lead collisions at $\sqrt{s_{NN}} = 5.02$ TeV”, *Phys. Lett. B* **803** (2020) 135328, arXiv:1906.03322 [hep-ex].
- [29] ALICE Collaboration, S. Acharya *et al.*, “Measurement of the production cross section of prompt Ξ_c^0 baryons at midrapidity in pp collisions at $\sqrt{s} = 5.02$ TeV”, *JHEP* **10** (2021) 159, arXiv:2105.05616 [nucl-ex].

- [30] **ALICE** Collaboration, S. Acharya *et al.*, “Measurement of Prompt D^0 , Λ_c^+ , and $\Sigma_c^{0,++}(2455)$ Production in Proton–Proton Collisions at $\sqrt{s} = 13$ TeV”, *Phys. Rev. Lett.* **128** (2022) 012001, arXiv:2106.08278 [hep-ex].
- [31] **ALICE** Collaboration, S. Acharya *et al.*, “First measurement of Ω_c^0 production in pp collisions at $\sqrt{s} = 13$ TeV”, *Phys. Lett. B* **846** (2023) 137625, arXiv:2205.13993 [nucl-ex].
- [32] **LHCb** Collaboration, R. Aaij *et al.*, “Prompt Λ_c^+ production in pPb collisions at $\sqrt{s_{NN}} = 5.02$ TeV”, *JHEP* **02** (2019) 102, arXiv:1809.01404 [hep-ex].
- [33] **LHCb** Collaboration, R. Aaij *et al.*, “Measurement of b hadron fractions in 13 TeV pp collisions”, *Phys. Rev. D* **100** (2019) 031102, arXiv:1902.06794 [hep-ex].
- [34] **LHCb** Collaboration, R. Aaij *et al.*, “Study of the production of Λ_b^0 and \bar{B}^0 hadrons in pp collisions and first measurement of the $\Lambda_b^0 \rightarrow J/\psi p K^-$ branching fraction”, *Chin. Phys. C* **40** (2016) 011001, arXiv:1509.00292 [hep-ex].
- [35] **LHCb** Collaboration, R. Aaij *et al.*, “Measurement of B^+ , B^0 and Λ_b^0 production in pPb collisions at $\sqrt{s_{NN}} = 8.16$ TeV”, *Phys. Rev. D* **99** (2019) 052011, arXiv:1902.05599 [hep-ex].
- [36] **ALICE** Collaboration, S. Acharya *et al.*, “Study of flavor dependence of the baryon-to-meson ratio in proton-proton collisions at $\sqrt{s} = 13$ TeV”, *Phys. Rev. D* **108** (2023) 112003, arXiv:2308.04873 [hep-ex].
- [37] **ALICE** Collaboration, S. Acharya *et al.*, “Charm-quark fragmentation fractions and production cross section at midrapidity in pp collisions at the LHC”, *Phys. Rev. D* **105** (2022) L011103, arXiv:2105.06335 [nucl-ex].
- [38] **LHCb** Collaboration, R. Aaij *et al.*, “Measurement of Ξ_c^+ production in pPb collisions at $s_{NN}=8.16$ TeV at LHCb”, *Phys. Rev. C* **109** (2024) 044901, arXiv:2305.06711 [hep-ex].
- [39] J. Altmann, A. Dubla, V. Greco, A. Rossi, and P. Skands, “Towards the understanding of heavy quarks hadronization: from leptonic to heavy-ion collisions”, arXiv:2405.19137 [hep-ph].
- [40] V. Minissale, S. Plumari, and V. Greco, “Charm hadrons in pp collisions at LHC energy within a coalescence plus fragmentation approach”, *Phys. Lett. B* **821** (2021) 136622, arXiv:2012.12001 [hep-ph].
- [41] V. Minissale, V. Greco, and S. Plumari, “Bottomed mesons and baryons in pp collisions at $\sqrt{s} = 5$ TeV LHC energy within a Coalescence plus Fragmentation approach”, arXiv:2405.19244 [hep-ph].
- [42] J. Song, H.-h. Li, and F.-l. Shao, “New feature of low p_T charm quark hadronization in pp collisions at $\sqrt{s} = 7$ TeV”, *Eur. Phys. J. C* **78** (2018) 344, arXiv:1801.09402 [hep-ph].
- [43] A. Beraudo, A. De Pace, D. Pablos, F. Prino, M. Monteno, and M. Nardi, “Heavy-flavor transport and hadronization in pp collisions”, *Phys. Rev. D* **109** (2024) L011501, arXiv:2306.02152 [hep-ph].
- [44] A. Andronic, P. Braun-Munzinger, M. K. Köhler, A. Mazeliauskas, K. Redlich, J. Stachel, and V. Vislavicius, “The multiple-charm hierarchy in the statistical hadronization model”, *JHEP* **07** (2021) 035, arXiv:2104.12754 [hep-ph].
- [45] M. He and R. Rapp, “Charm-Baryon Production in Proton-Proton Collisions”, *Phys. Lett. B* **795** (2019) 117–121, arXiv:1902.08889 [nucl-th].

- [46] M. He and R. Rapp, “Bottom Hadrochemistry in High-Energy Hadronic Collisions”, *Phys. Rev. Lett.* **131** (2023) 012301, arXiv:2209.13419 [hep-ph].
- [47] J. R. Christiansen and P. Z. Skands, “String Formation Beyond Leading Colour”, *JHEP* **08** (2015) 003, arXiv:1505.01681 [hep-ph].
- [48] C. Bierlich, G. Gustafson, L. Lönnblad, and H. Shah, “The dynamic hadronization of charm quarks in heavy-ion collisions”, *Eur. Phys. J. C* **84** (2024) 231, arXiv:2309.12452 [hep-ph].
- [49] M. Arneodo, “Nuclear effects in structure functions”, *Phys. Rept.* **240** (1994) 301–393.
- [50] S. Malace, D. Gaskell, D. W. Higinbotham, and I. Cloet, “The Challenge of the EMC Effect: existing data and future directions”, *Int. J. Mod. Phys. E* **23** (2014) 1430013, arXiv:1405.1270 [nucl-ex].
- [51] K. J. Eskola, H. Paukkunen, and C. A. Salgado, “EPS09: A New Generation of NLO and LO Nuclear Parton Distribution Functions”, *JHEP* **04** (2009) 065, arXiv:0902.4154 [hep-ph].
- [52] M. Hirai, S. Kumano, and T. H. Nagai, “Determination of nuclear parton distribution functions and their uncertainties in next-to-leading order”, *Phys. Rev. C* **76** (2007) 065207, arXiv:0709.3038 [hep-ph].
- [53] D. de Florian and R. Sassot, “Nuclear parton distributions at next-to-leading order”, *Phys. Rev. D* **69** (2004) 074028, arXiv:hep-ph/0311227.
- [54] K. J. Eskola, P. Paakkinen, H. Paukkunen, and C. A. Salgado, “EPPS16: Nuclear parton distributions with LHC data”, *Eur. Phys. J. C* **77** (2017) 163, arXiv:1612.05741 [hep-ph].
- [55] I. Vitev, “Non-Abelian energy loss in cold nuclear matter”, *Phys. Rev. C* **75** (2007) 064906, arXiv:hep-ph/0703002.
- [56] X.-N. Wang, “Systematic study of high p_T hadron spectra in pp , pA and AA collisions from SPS to RHIC energies”, *Phys. Rev. C* **61** (2000) 064910, arXiv:nucl-th/9812021.
- [57] B. Z. Kopeliovich, J. Nemchik, A. Schafer, and A. V. Tarasov, “Cronin effect in hadron production off nuclei”, *Phys. Rev. Lett.* **88** (2002) 232303, arXiv:hep-ph/0201010.
- [58] A. Kusina, J.-P. Lansberg, I. Schienbein, and H.-S. Shao, “Gluon Shadowing in Heavy-Flavor Production at the LHC”, *Phys. Rev. Lett.* **121** (2018) 052004, arXiv:1712.07024 [hep-ph].
- [59] K. J. Eskola, I. Helenius, P. Paakkinen, and H. Paukkunen, “A QCD analysis of LHCb D-meson data in p+Pb collisions”, *JHEP* **05** (2020) 037, arXiv:1906.02512 [hep-ph].
- [60] ALICE Collaboration, B. B. Abelev *et al.*, “Multiplicity dependence of pion, kaon, proton and lambda production in p-Pb collisions at $\sqrt{s_{NN}} = 5.02$ TeV”, *Phys. Lett. B* **728** (2014) 25–38, arXiv:1307.6796 [nucl-ex].
- [61] CMS Collaboration, S. Chatrchyan *et al.*, “Study of the Production of Charged Pions, Kaons, and Protons in pPb Collisions at $\sqrt{s_{NN}} = 5.02$ TeV”, *Eur. Phys. J. C* **74** (2014) 2847, arXiv:1307.3442 [hep-ex].
- [62] E. Schnedermann, J. Sollfrank, and U. Heinz, “Thermal phenomenology of hadrons from 200-AGeV S+S collisions”, *Phys. Rev. C* **48** (1993) 2462–2475, arXiv:nucl-th/9307020.
- [63] R. J. Fries *et al.*, “Hadronization in heavy ion collisions: Recombination and fragmentation of partons”, *Phys. Rev. Lett.* **90** (2003) 202303, arXiv:nucl-th/0301087.

- [64] **ALICE** Collaboration, S. Acharya *et al.*, “Measurement of prompt D^0 , D^+ , D^{*+} , and D_S^+ production in p–Pb collisions at $\sqrt{s_{NN}} = 5.02$ TeV”, *JHEP* **12** (2019) 092, arXiv:1906.03425 [nucl-ex].
- [65] **CMS** Collaboration, V. Khachatryan *et al.*, “Study of B Meson Production in p+Pb Collisions at $\sqrt{s_{NN}} = 5.02$ TeV Using Exclusive Hadronic Decays”, *Phys. Rev. Lett.* **116** (2016) 032301, arXiv:1508.06678 [nucl-ex].
- [66] S. Frixione, P. Nason, and G. Ridolfi, “A Positive-weight next-to-leading-order Monte Carlo for heavy flavour hadroproduction”, *JHEP* **09** (2007) 126, arXiv:0707.3088 [hep-ph].
- [67] T. Sjostrand, S. Mrenna, and P. Z. Skands, “PYTHIA 6.4 Physics and Manual”, *JHEP* **05** (2006) 026, arXiv:hep-ph/0603175.
- [68] **ALICE** Collaboration, K. Aamodt *et al.*, “The ALICE experiment at the CERN LHC”, *JINST* **3** (2008) S08002.
- [69] **ALICE** Collaboration, B. B. Abelev *et al.*, “Performance of the ALICE Experiment at the CERN LHC”, *Int. J. Mod. Phys. A* **29** (2014) 1430044, arXiv:1402.4476 [nucl-ex].
- [70] **ALICE** Collaboration, B. Abelev *et al.*, “Technical Design Report for the Upgrade of the ALICE Inner Tracking System”, *J. Phys. G* **41** (2014) 087002.
- [71] J. Alme *et al.*, “The ALICE TPC, a large 3-dimensional tracking device with fast readout for ultra-high multiplicity events”, *Nucl. Instr. Meth. A* **622** (2010) 316–367, arXiv:1001.1950 [physics.ins-det].
- [72] A. Akindinov *et al.*, “Performance of the ALICE Time-Of-Flight detector at the LHC”, *Eur. Phys. J. Plus* **128** (2013) 44.
- [73] **ALICE** Collaboration, E. Abbas *et al.*, “Performance of the ALICE VZERO system”, *JINST* **8** (2013) P10016, arXiv:1306.3130 [nucl-ex].
- [74] **ALICE** Collaboration, B. B. Abelev *et al.*, “Measurement of visible cross sections in proton-lead collisions at $\sqrt{s_{NN}} = 5.02$ TeV in van der Meer scans with the ALICE detector”, *JINST* **9** (2014) P11003, arXiv:1405.1849 [nucl-ex].
- [75] **Particle Data Group** Collaboration, R. L. Workman *et al.*, “Review of Particle Physics”, *PTEP* **2022** (2022) 083C01.
- [76] I. Kisel, I. Kulakov, and M. Zyzak, “Standalone first level event selection package for the CBM Experiment”, *IEEE Transactions on Nuclear Science* **60** (2013) 3703–3708.
- [77] T. Chen and C. Guestrin, “XGBoost: A Scalable Tree Boosting System”, arXiv:1603.02754 [cs.LG].
- [78] L. Barioglio, F. Catalano, M. Concas, P. Fecchio, F. Grosa, F. Mazzaschi, and M. Puccio, “hipe4ml/hipe4ml”, Nov., 2021. <https://doi.org/10.5281/zenodo.5734093>.
- [79] X.-N. Wang and M. Gyulassy, “HIJING: A Monte Carlo model for multiple jet production in pp, pA, and AA collisions”, *Physical Review D* **44** (1991) 3501.
- [80] **ALICE** Collaboration, S. Acharya *et al.*, “Measurement of the non-prompt D-meson fraction as a function of multiplicity in proton-proton collisions at $\sqrt{s} = 13$ TeV”, *JHEP* **10** (2023) 092, arXiv:2302.07783 [nucl-ex].

- [81] M. Cacciari, S. Frixione, and P. Nason, “The p(T) spectrum in heavy flavor photoproduction”, *JHEP* **03** (2001) 006, arXiv:hep-ph/0102134.
- [82] J. Pumplin, D. R. Stump, J. Huston, H. L. Lai, P. M. Nadolsky, and W. K. Tung, “New generation of parton distributions with uncertainties from global QCD analysis”, *JHEP* **07** (2002) 012, arXiv:hep-ph/0201195.
- [83] **Particle Data Group** Collaboration, M. Tanabashi *et al.*, “Review of Particle Physics”, *Phys. Rev. D* **98** (2018) 030001.
- [84] D. J. Lange, “The EvtGen particle decay simulation package”, *Nucl. Instrum. Meth. A* **462** (2001) 152–155.
- [85] **ALICE** Collaboration, S. Acharya *et al.*, “Measurement of D^0 , D^+ , D^{*+} and D_s^+ production in pp collisions at $\sqrt{s} = 5.02$ TeV with ALICE”, *Eur. Phys. J. C* **79** (2019) 388, arXiv:1901.07979 [nucl-ex].
- [86] **LHCb** Collaboration, R. Aaij *et al.*, “Measurement of the B^\pm production cross-section in pp collisions at $\sqrt{s} = 7$ and 13 TeV”, *JHEP* **12** (2017) 026, arXiv:1710.04921 [hep-ex].
- [87] **ALICE** Collaboration, S. Acharya *et al.*, “Measurement of beauty-quark production in pp collisions at $\sqrt{s} = 13$ TeV via non-prompt D mesons”, arXiv:2402.16417 [hep-ex].
- [88] **ALICE** Collaboration, S. Acharya *et al.*, “Inclusive, prompt and non-prompt J/ψ production at midrapidity in p-Pb collisions at $\sqrt{s_{NN}} = 5.02$ TeV”, *JHEP* **06** (2022) 011, arXiv:2105.04957 [nucl-ex].
- [89] **LHCb** Collaboration, R. Aaij *et al.*, “Prompt and nonprompt J/ψ production and nuclear modification in pPb collisions at $\sqrt{s_{NN}} = 8.16$ TeV”, *Phys. Lett. B* **774** (2017) 159–178, arXiv:1706.07122 [hep-ex].
- [90] H.-S. Shao, “HELAC-Onia: An automatic matrix element generator for heavy quarkonium physics”, *Comput. Phys. Commun.* **184** (2013) 2562–2570, arXiv:1212.5293 [hep-ph].
- [91] H.-S. Shao, “HELAC-Onia 2.0: an upgraded matrix-element and event generator for heavy quarkonium physics”, *Comput. Phys. Commun.* **198** (2016) 238–259, arXiv:1507.03435 [hep-ph].
- [92] J.-P. Lansberg and H.-S. Shao, “Towards an automated tool to evaluate the impact of the nuclear modification of the gluon density on quarkonium, D and B meson production in proton–nucleus collisions”, *Eur. Phys. J. C* **77** (2017) 1, arXiv:1610.05382 [hep-ph].
- [93] K. Kovarik *et al.*, “nCTEQ15 - Global analysis of nuclear parton distributions with uncertainties in the CTEQ framework”, *Phys. Rev. D* **93** (2016) 085037, arXiv:1509.00792 [hep-ph].
- [94] **LHCb** Collaboration, R. Aaij *et al.*, “Measurement of J/ψ production in pp collisions at $\sqrt{s} = 7$ TeV”, *Eur. Phys. J. C* **71** (2011) 1645, arXiv:1103.0423 [hep-ex].
- [95] **CMS** Collaboration, V. Khachatryan *et al.*, “Measurement of J/ψ and $\psi(2S)$ Prompt Double-Differential Cross Sections in pp Collisions at $\sqrt{s}=7$ TeV”, *Phys. Rev. Lett.* **114** (2015) 191802, arXiv:1502.04155 [hep-ex].
- [96] **ALICE** Collaboration, S. Acharya *et al.*, “Prompt D^0 , D^+ , and D^{*+} production in Pb–Pb collisions at $\sqrt{s_{NN}} = 5.02$ TeV”, *JHEP* **01** (2022) 174, arXiv:2110.09420 [nucl-ex].












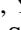
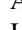


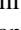


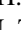



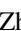
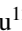
- [97] **ALICE** Collaboration, S. Acharya *et al.*, “Measurement of beauty production via non-prompt D^0 mesons in Pb-Pb collisions at $\sqrt{s_{NN}} = 5.02$ TeV”, *JHEP* **12** (2022) 126, arXiv:2202.00815 [nucl-ex].
- [98] **ALICE** Collaboration, S. Acharya *et al.*, “Measurement of the production cross section of prompt Ξ_c^0 baryons in p–Pb collisions at $\sqrt{s_{NN}} = 5.02$ TeV”, arXiv:2405.14538 [nucl-ex].
- [99] **CMS** Collaboration, A. M. Sirunyan *et al.*, “Strange hadron production in pp and pPb collisions at $\sqrt{s_{NN}} = 5.02$ TeV”, *Phys. Rev. C* **101** (2020) 064906, arXiv:1910.04812 [hep-ex].
- [100] T. Pierog *et al.*, “EPOS LHC: Test of collective hadronization with data measured at the CERN Large Hadron Collider”, *Phys. Rev. C* **92** (2015) 034906, arXiv:1306.0121 [hep-ph].

A The ALICE Collaboration

S. Acharya ¹²⁷, D. Adamová ⁸⁶, A. Agarwal¹³⁵, G. Aglieri Rinella ³², L. Aglietta²⁴, M. Agnello ²⁹, N. Agrawal ²⁵, Z. Ahammed ¹³⁵, S. Ahmad ¹⁵, S.U. Ahn ⁷¹, I. Ahuja ³⁷, A. Akindinov ¹⁴¹, V. Akishina³⁸, M. Al-Turany ⁹⁷, D. Aleksandrov ¹⁴¹, B. Alessandro ⁵⁶, H.M. Alfanda ⁶, R. Alfaro Molina ⁶⁷, B. Ali ¹⁵, A. Alici ²⁵, N. Alizadehvandchali ¹¹⁶, A. Alkin ¹⁰⁴, J. Alme ²⁰, G. Alocco ⁵², T. Alt ⁶⁴, A.R. Altamura ⁵⁰, I. Altsybeev ⁹⁵, J.R. Alvarado ⁴⁴, C.O.R. Alvarez⁴⁴, M.N. Anaam ⁶, C. Andrei ⁴⁵, N. Andreou ¹¹⁵, A. Andronic ¹²⁶, E. Andronov ¹⁴¹, V. Anguelov ⁹⁴, F. Antinori ⁵⁴, P. Antonioli ⁵¹, N. Apadula ⁷⁴, L. Aphecetche ¹⁰³, H. Appelshäuser ⁶⁴, C. Arata ⁷³, S. Arcelli ²⁵, R. Arnaldi ⁵⁶, J.G.M.C.A. Arneiro ¹¹⁰, I.C. Arsene ¹⁹, M. Arslanok ¹³⁸, A. Augustinus ³², R. Averbeck ⁹⁷, D. Averyanov ¹⁴¹, M.D. Azmi ¹⁵, H. Baba¹²⁴, A. Badalà ⁵³, J. Bae ¹⁰⁴, Y.W. Baek ⁴⁰, X. Bai ¹²⁰, R. Bailhache ⁶⁴, Y. Bailung ⁴⁸, R. Bala ⁹¹, A. Balbino ²⁹, A. Baldisseri ¹³⁰, B. Balis ², D. Banerjee ⁴, Z. Banoo ⁹¹, V. Barbasova³⁷, F. Barile ³¹, L. Barioglio ⁵⁶, M. Barlou⁷⁸, B. Barman⁴¹, G.G. Barnaföldi ⁴⁶, L.S. Barnby ¹¹⁵, E. Barreau ¹⁰³, V. Barret ¹²⁷, L. Barreto ¹¹⁰, C. Bartels ¹¹⁹, K. Barth ³², E. Bartsch ⁶⁴, N. Bastid ¹²⁷, S. Basu ⁷⁵, G. Batigne ¹⁰³, D. Battistini ⁹⁵, B. Batyunya ¹⁴², D. Bauri⁴⁷, J.L. Bazo Alba ¹⁰¹, I.G. Bearden ⁸³, C. Beattie ¹³⁸, P. Becht ⁹⁷, D. Behera ⁴⁸, I. Belikov ¹²⁹, A.D.C. Bell Hechavarria ¹²⁶, F. Bellini ²⁵, R. Bellwied ¹¹⁶, S. Belokurova ¹⁴¹, L.G.E. Beltran ¹⁰⁹, Y.A.V. Beltran ⁴⁴, G. Bencedi ⁴⁶, A. Bensaoula¹¹⁶, S. Beole ²⁴, Y. Berdnikov ¹⁴¹, A. Berdnikova ⁹⁴, L. Bergmann ⁹⁴, M.G. Besoiu ⁶³, L. Betev ³², P.P. Bhaduri ¹³⁵, A. Bhasin ⁹¹, B. Bhattacharjee ⁴¹, L. Bianchi ²⁴, J. Bielčik ³⁵, J. Bielčíková ⁸⁶, A.P. Bigot ¹²⁹, A. Bilandzic ⁹⁵, G. Biro ⁴⁶, S. Biswas ⁴, N. Bize ¹⁰³, J.T. Blair ¹⁰⁸, D. Blau ¹⁴¹, M.B. Blidaru ⁹⁷, N. Bluhme³⁸, C. Blume ⁶⁴, G. Boca ^{21,55}, F. Bock ⁸⁷, T. Bodova ²⁰, J. Bok ¹⁶, L. Boldizsár ⁴⁶, M. Bombara ³⁷, P.M. Bond ³², G. Bonomi ^{134,55}, H. Borel ¹³⁰, A. Borissov ¹⁴¹, A.G. Borquez Carcamo ⁹⁴, E. Botta ²⁴, Y.E.M. Bouziani ⁶⁴, L. Bratrud ⁶⁴, P. Braun-Munzinger ⁹⁷, M. Bregant ¹¹⁰, M. Broz ³⁵, G.E. Bruno ^{96,31}, V.D. Buchakchiev ³⁶, M.D. Buckland ⁸⁵, D. Budnikov ¹⁴¹, H. Buesching ⁶⁴, S. Bufalino ²⁹, P. Buhler ¹⁰², N. Burmasov ¹⁴¹, Z. Buthelezi ^{68,123}, A. Bylinkin ²⁰, S.A. Bysiak¹⁰⁷, J.C. Cabanillas Noris ¹⁰⁹, M.F.T. Cabrera¹¹⁶, M. Cai ⁶, H. Caines ¹³⁸, A. Caliva ²⁸, E. Calvo Villar ¹⁰¹, J.M.M. Camacho ¹⁰⁹, P. Camerini ²³, F.D.M. Canedo ¹¹⁰, S.L. Cantway ¹³⁸, M. Carabas ¹¹³, A.A. Carballo ³², F. Carnesecchi ³², R. Caron ¹²⁸, L.A.D. Carvalho ¹¹⁰, J. Castillo Castellanos ¹³⁰, M. Castoldi ³², F. Catalano ³², S. Cattaruzzi ²³, C. Ceballos Sanchez ¹⁴², R. Cerri²⁴, I. Chakaberia ⁷⁴, P. Chakraborty ¹³⁶, S. Chandra ¹³⁵, S. Chapeland ³², M. Chartier ¹¹⁹, S. Chattopadhyay¹³⁵, S. Chattopadhyay ¹³⁵, S. Chattopadhyay ⁹⁹, M. Chen³⁹, T. Cheng ^{97,6}, C. Cheshkov ¹²⁸, V. Chibante Barroso ³², D.D. Chinellato ¹¹¹, E.S. Chizzali ^{119,95}, J. Cho ⁵⁸, S. Cho ⁵⁸, P. Chochula ³², Z.A. Chochulska¹³⁶, D. Choudhury⁴¹, P. Christakoglou ⁸⁴, C.H. Christensen ⁸³, P. Christiansen ⁷⁵, T. Chujo ¹²⁵, M. Ciaccio ²⁹, C. Cicalo ⁵², M.R. Ciupek⁹⁷, G. Clai^{III,51}, F. Colamaria ⁵⁰, J.S. Colburn¹⁰⁰, D. Colella ³¹, M. Colocci ²⁵, M. Concas ³², G. Conesa Balbastre ⁷³, Z. Conesa del Valle ¹³¹, G. Contin ²³, J.G. Contreras ³⁵, M.L. Coquet ¹⁰³, P. Cortese ^{133,56}, M.R. Cosentino ¹¹², F. Costa ³², S. Costanza ^{21,55}, C. Cot ¹³¹, P. Crochet ¹²⁷, R. Cruz-Torres ⁷⁴, P. Cui ⁶, M.M. Czarnynoga¹³⁶, A. Dainese ⁵⁴, G. Dange³⁸, M.C. Danisch ⁹⁴, A. Danu ⁶³, P. Das ⁸⁰, P. Das ⁴, S. Das ⁴, A.R. Dash ¹²⁶, S. Dash ⁴⁷, A. De Caro ²⁸, G. de Cataldo ⁵⁰, J. de Cuveland³⁸, A. De Falco ²², D. De Gruttola ²⁸, N. De Marco ⁵⁶, C. De Martin ²³, S. De Pasquale ²⁸, R. Deb ¹³⁴, R. Del Grande ⁹⁵, L. Dello Stritto ³², W. Deng ⁶, K.C. Devereaux¹⁸, P. Dhankher ¹⁸, D. Di Bari ³¹, A. Di Mauro ³², B. Diab ¹³⁰, R.A. Diaz ^{142,7}, T. Dietel ¹¹⁴, Y. Ding ⁶, J. Ditzel ⁶⁴, R. Divià ³², Ø. Djuvsland²⁰, U. Dmitrieva ¹⁴¹, A. Dobrin ⁶³, B. Dönigus ⁶⁴, J.M. Dubinski ¹³⁶, A. Dubla ⁹⁷, P. Dupieux ¹²⁷, N. Dzalaiova¹³, T.M. Eder ¹²⁶, R.J. Ehlers ⁷⁴, F. Eisenhut ⁶⁴, R. Ejima⁹², D. Elia ⁵⁰, B. Erazmus ¹⁰³, F. Ercolessi ²⁵, B. Espagnon ¹³¹, G. Eulisse ³², D. Evans ¹⁰⁰, S. Evdokimov ¹⁴¹, L. Fabbietti ⁹⁵, M. Faggin ²³, J. Faivre ⁷³, F. Fan ⁶, W. Fan ⁷⁴, A. Fantoni ⁴⁹, M. Fasel ⁸⁷, A. Feliciello ⁵⁶, G. Feofilov ¹⁴¹, A. Fernández Téllez ⁴⁴, L. Ferrandi ¹¹⁰, M.B. Ferrer ³², A. Ferrero ¹³⁰, C. Ferrero ^{IV,56}, A. Ferretti ²⁴, V.J.G. Feuillard ⁹⁴, V. Filova ³⁵, D. Finogeev ¹⁴¹, F.M. Fionda ⁵², E. Flatland³², F. Flor ^{138,116}, A.N. Flores ¹⁰⁸, S. Foertsch ⁶⁸, I. Fokin ⁹⁴, S. Fokin ¹⁴¹, U. Follo^{IV,56}, E. Fragiaco ⁵⁷, E. Frajna ⁴⁶, U. Fuchs ³², N. Funicello ²⁸, C. Furget ⁷³, A. Furs ¹⁴¹, T. Fusayasu ⁹⁸, J.J. Gaardhøje ⁸³, M. Gagliardi ²⁴, A.M. Gago ¹⁰¹, T. Gahlaut⁴⁷, C.D. Galvan ¹⁰⁹, D.R. Gangadharan ¹¹⁶, P. Ganoti ⁷⁸, C. Garabatos ⁹⁷, J.M. García⁴⁴, T. García Chávez ⁴⁴, E. García-Solis ⁹, C. Gargiulo ³², P. Gasik ⁹⁷, H.M. Gaur³⁸, A. Gautam ¹¹⁸, M.B. Gay Ducati ⁶⁶, M. Germain ¹⁰³, R.A. Gernhaeuser⁹⁵, C. Ghosh¹³⁵, M. Giacalone ⁵¹, G. Gioachin ²⁹, S.K. Giri¹³⁵, P. Giubellino ^{97,56}, P. Giubilato ²⁷, A.M.C. Glaenger ¹³⁰, P. Glässel ⁹⁴, E. Glimos ¹²², D.J.Q. Goh⁷⁶, V. Gonzalez ¹³⁷, P. Gordeev ¹⁴¹, M. Gorgon ², K. Goswami ⁴⁸, S. Gotovac³³, V. Grabski ⁶⁷, L.K. Graczykowski ¹³⁶, E. Grecka ⁸⁶, A. Grelli ⁵⁹,

C. Grigoras ³², V. Grigoriev ¹⁴¹, S. Grigoryan ^{142,1}, F. Grosa ³², J.F. Grosse-Oetringhaus ³², R. Grosso ⁹⁷, D. Grund ³⁵, N.A. Grunwald⁹⁴, G.G. Guardiano ¹¹¹, R. Guernane ⁷³, M. Guilbaud ¹⁰³, K. Gulbrandsen ⁸³, J.J.W.K. Gumprecht¹⁰², T. Gündem ⁶⁴, T. Gunji ¹²⁴, W. Guo ⁶, A. Gupta ⁹¹, R. Gupta ⁹¹, R. Gupta ⁴⁸, K. Gwizdziel ¹³⁶, L. Gyulai ⁴⁶, C. Hadjidakis ¹³¹, F.U. Haider ⁹¹, S. Haidlova ³⁵, M. Haldar⁴, H. Hamagaki ⁷⁶, Y. Han ¹³⁹, B.G. Hanley ¹³⁷, R. Hannigan ¹⁰⁸, J. Hansen ⁷⁵, M.R. Haque ⁹⁷, J.W. Harris ¹³⁸, A. Harton ⁹, M.V. Hartung ⁶⁴, H. Hassan ¹¹⁷, D. Hatzifotiadou ⁵¹, P. Hauer ⁴², L.B. Havener ¹³⁸, E. Hellbär ⁹⁷, H. Helstrup ³⁴, M. Hemmer ⁶⁴, T. Herman ³⁵, S.G. Hernandez¹¹⁶, G. Herrera Corral ⁸, S. Herrmann ¹²⁸, K.F. Hetland ³⁴, B. Heybeck ⁶⁴, H. Hillemanns ³², B. Hippolyte ¹²⁹, I.P.M. Hobus⁸⁴, F.W. Hoffmann ⁷⁰, B. Hofman ⁵⁹, G.H. Hong ¹³⁹, M. Horst ⁹⁵, A. Horzyk ², Y. Hou ⁶, P. Hristov ³², P. Huhn⁶⁴, L.M. Huhta ¹¹⁷, T.J. Humanic ⁸⁸, A. Hutson ¹¹⁶, D. Hutter ³⁸, M.C. Hwang ¹⁸, R. Ilkaev¹⁴¹, M. Inaba ¹²⁵, G.M. Innocenti ³², M. Ippolitov ¹⁴¹, A. Isakov ⁸⁴, T. Isidori ¹¹⁸, M.S. Islam ⁹⁹, S. Iurchenko¹⁴¹, M. Ivanov ⁹⁷, M. Ivanov¹³, V. Ivanov ¹⁴¹, K.E. Iversen ⁷⁵, M. Jablonski ², B. Jacak ^{18,74}, N. Jacazio ²⁵, P.M. Jacobs ⁷⁴, S. Jadlovská¹⁰⁶, J. Jadlovsky¹⁰⁶, S. Jaelani ⁸², C. Jahnke ¹¹⁰, M.J. Jakubowska ¹³⁶, M.A. Janik ¹³⁶, T. Janson⁷⁰, S. Ji ¹⁶, S. Jia ¹⁰, T. Jiang ¹⁰, A.A.P. Jimenez ⁶⁵, F. Jonas ⁷⁴, D.M. Jones ¹¹⁹, J.M. Jowett ^{32,97}, J. Jung ⁶⁴, M. Jung ⁶⁴, A. Junique ³², A. Jusko ¹⁰⁰, J. Kaewjai¹⁰⁵, P. Kalinak ⁶⁰, A. Kalweit ³², A. Karasu Uysal ⁷², D. Karatovic ⁸⁹, N. Karatzenis¹⁰⁰, O. Karavichev ¹⁴¹, T. Karavicheva ¹⁴¹, E. Karpechev ¹⁴¹, M.J. Karwowska ^{32,136}, U. Keschull ⁷⁰, R. Keidel ¹⁴⁰, M. Keil ³², B. Ketzer ⁴², S.S. Khade ⁴⁸, A.M. Khan ¹²⁰, S. Khan ¹⁵, A. Khanzadeev ¹⁴¹, Y. Kharlov ¹⁴¹, A. Khatun ¹¹⁸, A. Khuntia ³⁵, Z. Khuranova ⁶⁴, B. Kileng ³⁴, B. Kim ¹⁰⁴, C. Kim ¹⁶, D.J. Kim ¹¹⁷, E.J. Kim ⁶⁹, J. Kim ¹³⁹, J. Kim ⁵⁸, J. Kim ^{32,69}, M. Kim ¹⁸, S. Kim ¹⁷, T. Kim ¹³⁹, K. Kimura ⁹², A. Kirkova³⁶, S. Kirsch ⁶⁴, I. Kisel ³⁸, S. Kiselev ¹⁴¹, A. Kisiel ¹³⁶, J.P. Kitowski ², J.L. Klay ⁵, J. Klein ³², S. Klein ⁷⁴, C. Klein-Bösing ¹²⁶, M. Kleiner ⁶⁴, T. Klemenz ⁹⁵, A. Kluge ³², C. Kobdaj ¹⁰⁵, R. Kohara¹²⁴, T. Kollegger⁹⁷, A. Kondratyev ¹⁴², N. Kondratyeva ¹⁴¹, J. König ⁶⁴, S.A. Königstorfer ⁹⁵, P.J. Konopka ³², G. Kornakov ¹³⁶, M. Korwieser ⁹⁵, S.D. Koryciak ², C. Koster⁸⁴, A. Kotliarov ⁸⁶, N. Kovacic⁸⁹, V. Kovalenko ¹⁴¹, M. Kowalski ¹⁰⁷, V. Kozuharov ³⁶, G. Kozlov³⁸, I. Králik ⁶⁰, A. Kravčáková ³⁷, L. Krcal ^{32,38}, M. Krivda ^{100,60}, F. Krizek ⁸⁶, K. Krizkova Gajdosova ³², C. Krug ⁶⁶, M. Krüger ⁶⁴, D.M. Krupova ³⁵, E. Kryshen ¹⁴¹, V. Kučera ⁵⁸, C. Kuhn ¹²⁹, P.G. Kuijjer ⁸⁴, T. Kumaoka¹²⁵, D. Kumar¹³⁵, L. Kumar ⁹⁰, N. Kumar⁹⁰, S. Kumar ⁵⁰, S. Kundu ³², P. Kurashvili ⁷⁹, A. Kurepin ¹⁴¹, A.B. Kurepin ¹⁴¹, A. Kuryakin ¹⁴¹, S. Kushpil ⁸⁶, V. Kuskov ¹⁴¹, M. Kutyla¹³⁶, A. Kuznetsov¹⁴², M.J. Kweon ⁵⁸, Y. Kwon ¹³⁹, S.L. La Pointe ³⁸, P. La Rocca ²⁶, A. Lakrathok¹⁰⁵, M. Lamanna ³², A.R. Landou ⁷³, R. Langoy ¹²¹, P. Larionov ³², E. Laudi ³², L. Lautner ^{32,95}, R.A.N. Laveaga¹⁰⁹, R. Lavicka ¹⁰², R. Lea ^{134,55}, H. Lee ¹⁰⁴, I. Legrand ⁴⁵, G. Legras ¹²⁶, J. Lehrbach ³⁸, A.M. Lejeune³⁵, T.M. Lelek², R.C. Lemmon ^{1,85}, I. León Monzón ¹⁰⁹, M.M. Lesch ⁹⁵, E.D. Lesser ¹⁸, P. Lévai ⁴⁶, M. Li⁶, X. Li¹⁰, B.E. Liang-gilman ¹⁸, J. Lien ¹²¹, R. Lietava ¹⁰⁰, I. Likmeta ¹¹⁶, B. Lim ²⁴, S.H. Lim ¹⁶, V. Lindenstruth ³⁸, A. Lindner⁴⁵, C. Lippmann ⁹⁷, D.H. Liu ⁶, J. Liu ¹¹⁹, G.S.S. Liveraro ¹¹¹, I.M. Lofnes ²⁰, C. Loizides ⁸⁷, S. Lokos ¹⁰⁷, J. Lömker ⁵⁹, X. Lopez ¹²⁷, E. López Torres ⁷, C. Lotteau¹²⁸, P. Lu ^{97,120}, Z. Lu ¹⁰, F.V. Lugo ⁶⁷, J.R. Luhder ¹²⁶, M. Lunardon ²⁷, G. Luparello ⁵⁷, Y.G. Ma ³⁹, M. Mager ³², A. Maire ¹²⁹, E.M. Majerz², M.V. Makariev ³⁶, M. Malaev ¹⁴¹, G. Malfattore ²⁵, N.M. Malik ⁹¹, Q.W. Malik¹⁹, S.K. Malik ⁹¹, L. Malinina ^{I,VIII,142}, D. Mallick ¹³¹, N. Mallick ⁴⁸, G. Mandaglio ^{30,53}, S.K. Mandal ⁷⁹, A. Manea ⁶³, V. Manko ¹⁴¹, F. Manso ¹²⁷, V. Manzari ⁵⁰, Y. Mao ⁶, R.W. Marcjan ², G.V. Margagliotti ²³, A. Margotti ⁵¹, A. Marín ⁹⁷, C. Markert ¹⁰⁸, P. Martinengo ³², M.I. Martínez ⁴⁴, G. Martínez García ¹⁰³, M.P.P. Martins ¹¹⁰, S. Masciocchi ⁹⁷, M. Masera ²⁴, A. Masoni ⁵², L. Massacrier ¹³¹, O. Massen ⁵⁹, A. Mastroserio ^{132,50}, O. Matonoha ⁷⁵, S. Mattiazzo ²⁷, A. Matyja ¹⁰⁷, A.L. Mazuecos ³², F. Mazzaschi ^{32,24}, M. Mazzilli ¹¹⁶, J.E. Mdhuli ¹²³, Y. Melikyan ⁴³, M. Melo ¹¹⁰, A. Menchaca-Rocha ⁶⁷, J.E.M. Mendez ⁶⁵, E. Meninno ¹⁰², A.S. Menon ¹¹⁶, M.W. Menzel^{32,94}, M. Meres ¹³, Y. Miake¹²⁵, L. Micheletti ³², D.L. Mihaylov ⁹⁵, K. Mikhaylov ^{142,141}, N. Minafra ¹¹⁸, D. Miśkowiec ⁹⁷, A. Modak ^{134,4}, B. Mohanty⁸⁰, M. Mohisin Khan ^{VI,15}, M.A. Molander ⁴³, S. Monira ¹³⁶, C. Mordasini ¹¹⁷, D.A. Moreira De Godoy ¹²⁶, I. Morozov ¹⁴¹, A. Morsch ³², T. Mrnjavac ³², V. Muccifora ⁴⁹, S. Muhuri ¹³⁵, J.D. Mulligan ⁷⁴, A. Mulliri ²², M.G. Munhoz ¹¹⁰, R.H. Munzer ⁶⁴, H. Murakami ¹²⁴, S. Murray ¹¹⁴, L. Musa ³², J. Musinsky ⁶⁰, J.W. Myrcha ¹³⁶, B. Naik ¹²³, A.I. Nambrath ¹⁸, B.K. Nandi ⁴⁷, R. Nania ⁵¹, E. Nappi ⁵⁰, A.F. Nassirpour ¹⁷, A. Nath ⁹⁴, S. Nath¹³⁵, C. Nattrass ¹²², M.N. Naydenov ³⁶, A. Neagu¹⁹, A. Negru¹¹³, E. Nekrasova¹⁴¹, L. Nellen ⁶⁵, R. Nepeivoda ⁷⁵, S. Nese ¹⁹, N. Nicassio ⁵⁰, B.S. Nielsen ⁸³, E.G. Nielsen ⁸³, S. Nikolaev ¹⁴¹, S. Nikulin ¹⁴¹, V. Nikulin ¹⁴¹, F. Noferini ⁵¹, S. Noh ¹², P. Nomokonov ¹⁴²,

J. Norman ¹¹⁹, N. Novitzky ⁸⁷, P. Nowakowski ¹³⁶, A. Nyanin ¹⁴¹, J. Nystrand ²⁰, S. Oh ¹⁷,
 A. Ohlson ⁷⁵, V.A. Okorokov ¹⁴¹, J. Oleniacz ¹³⁶, A. Onnerstad ¹¹⁷, C. Oppedisano ⁵⁶, A. Ortiz
 Velasquez ⁶⁵, J. Otwinowski ¹⁰⁷, M. Oya⁹², K. Oyama ⁷⁶, Y. Pachmayer ⁹⁴, S. Padhan ⁴⁷,
 D. Pagano ^{134,55}, G. Paic ⁶⁵, S. Paisano-Guzmán ⁴⁴, A. Palasciano ⁵⁰, S. Panebianco ¹³⁰,
 C. Pantouvakis²⁷, H. Park ¹²⁵, H. Park ¹⁰⁴, J. Park ¹²⁵, J.E. Parkkila ³², Y. Patley ⁴⁷, R.N. Patra⁵⁰,
 B. Paul ¹³⁵, H. Pei ⁶, T. Peitzmann ⁵⁹, X. Peng ¹¹, M. Pennisi ²⁴, S. Perciballi ²⁴, D. Peresunko ¹⁴¹,
 G.M. Perez ⁷, Y. Pestov¹⁴¹, M.T. Petersen⁸³, V. Petrov ¹⁴¹, M. Petrovici ⁴⁵, S. Piano ⁵⁷, M. Pikna ¹³,
 P. Pillot ¹⁰³, O. Pinazza ^{51,32}, L. Pinsky¹¹⁶, C. Pinto ⁹⁵, S. Pisano ⁴⁹, M. Płoskoń ⁷⁴, M. Planinic⁸⁹,
 F. Pliquet⁶⁴, D.K. Plociennik², M.G. Poghosyan ⁸⁷, B. Polichtchouk ¹⁴¹, S. Politano ²⁹, N. Poljak ⁸⁹,
 A. Pop ⁴⁵, S. Porteboeuf-Houssais ¹²⁷, V. Pozdniakov ^{1,142}, I.Y. Pozos ⁴⁴, K.K. Pradhan ⁴⁸,
 S.K. Prasad ⁴, S. Prasad ⁴⁸, R. Preghenella ⁵¹, F. Prino ⁵⁶, C.A. Pruneau ¹³⁷, I. Pshenichnov ¹⁴¹,
 M. Puccio ³², S. Pucillo ²⁴, S. Qiu ⁸⁴, L. Quaglia ²⁴, S. Ragoni ¹⁴, A. Rai ¹³⁸,
 A. Rakotozafindrabe ¹³⁰, L. Ramello ^{133,56}, F. Rami ¹²⁹, M. Rasa ²⁶, S.S. Räsänen ⁴³, R. Rath ⁵¹,
 M.P. Rauch ²⁰, I. Ravasenga ³², K.F. Read ^{87,122}, C. Reckziegel ¹¹², A.R. Redelbach ³⁸,
 K. Redlich ^{VII,79}, C.A. Reetz ⁹⁷, H.D. Regules-Medel⁴⁴, A. Rehman²⁰, F. Reidt ³², H.A. Reme-Ness ³⁴,
 Z. Rescakova³⁷, K. Reygers ⁹⁴, A. Riabov ¹⁴¹, V. Riabov ¹⁴¹, R. Ricci ²⁸, M. Richter ²⁰,
 A.A. Riedel ⁹⁵, W. Riegler ³², A.G. Riffero ²⁴, M. Rignanese²⁷, C. Ripoli²⁸, C. Ristea ⁶³,
 M.V. Rodriguez ³², M. Rodríguez Cahuantzi ⁴⁴, S.A. Rodríguez Ramírez ⁴⁴, K. Røed ¹⁹, R. Rogalev ¹⁴¹,
 E. Rogochaya ¹⁴², T.S. Rogoschinski ⁶⁴, D. Rohr ³², D. Röhrich ²⁰, S. Rojas Torres ³⁵, P.S. Rokita ¹³⁶,
 G. Romanenko ²⁵, F. Ronchetti ⁴⁹, E.D. Rosas⁶⁵, K. Roslon ¹³⁶, A. Rossi ⁵⁴, A. Roy ⁴⁸, S. Roy ⁴⁷,
 N. Rubini ^{51,25}, J.A. Rudolph⁸⁴, D. Ruggiano ¹³⁶, R. Rui ²³, P.G. Russek ², R. Russo ⁸⁴,
 A. Rustamov ⁸¹, E. Ryabinkin ¹⁴¹, Y. Ryabov ¹⁴¹, A. Rybicki ¹⁰⁷, J. Ryu ¹⁶, W. Rzesza ¹³⁶, B. Sabiu⁵¹,
 S. Sadovsky ¹⁴¹, J. Saetre ²⁰, K. Šafařík ³⁵, S.K. Saha ⁴, S. Saha ⁸⁰, B. Sahoo ⁴⁸, R. Sahoo ⁴⁸,
 S. Sahoo⁶¹, D. Sahu ⁴⁸, P.K. Sahu ⁶¹, J. Saini ¹³⁵, K. Sajdakova³⁷, S. Sakai ¹²⁵, M.P. Salvan ⁹⁷,
 S. Sambyal ⁹¹, D. Samitz ¹⁰², I. Sanna ^{32,95}, T.B. Saramela¹¹⁰, D. Sarkar ⁸³, P. Sarma ⁴¹, V. Sarritzu ²²,
 V.M. Sarti ⁹⁵, M.H.P. Sas ³², S. Sawan ⁸⁰, E. Scapparone ⁵¹, J. Schambach ⁸⁷, H.S. Scheid ⁶⁴,
 C. Schiaua ⁴⁵, R. Schicker ⁹⁴, F. Schlepper ⁹⁴, A. Schmah⁹⁷, C. Schmidt ⁹⁷, H.R. Schmidt⁹³,
 M.O. Schmidt ³², M. Schmidt⁹³, N.V. Schmidt ⁸⁷, A.R. Schmier ¹²², R. Schotter ¹²⁹, A. Schröter ³⁸,
 J. Schukraft ³², K. Schweda ⁹⁷, G. Scioli ²⁵, E. Scomarini ⁵⁶, J.E. Seger ¹⁴, Y. Sekiguchi¹²⁴,
 D. Sekihata ¹²⁴, M. Selina ⁸⁴, I. Selyuzhenkov ⁹⁷, S. Senyukov ¹²⁹, J.J. Seo ⁹⁴, D. Serebryakov ¹⁴¹,
 L. Serkin ⁶⁵, L. Šerkšnytė ⁹⁵, A. Sevcenco ⁶³, T.J. Shaba ⁶⁸, A. Shabetai ¹⁰³, R. Shahoyan³²,
 A. Shangaraev ¹⁴¹, B. Sharma ⁹¹, D. Sharma ⁴⁷, H. Sharma ⁵⁴, M. Sharma ⁹¹, S. Sharma ⁷⁶,
 S. Sharma ⁹¹, U. Sharma ⁹¹, A. Shatat ¹³¹, O. Sheibani¹¹⁶, K. Shigaki ⁹², M. Shimomura⁷⁷, J. Shin¹²,
 S. Shirinkin ¹⁴¹, Q. Shou ³⁹, Y. Sibiriak ¹⁴¹, S. Siddhanta ⁵², T. Siemiarczuk ⁷⁹, T.F. Silva ¹¹⁰,
 D. Silvermyr ⁷⁵, T. Simantathammakul¹⁰⁵, R. Simeonov ³⁶, B. Singh⁹¹, B. Singh ⁹⁵, K. Singh ⁴⁸,
 R. Singh ⁸⁰, R. Singh ⁹¹, R. Singh ⁹⁷, S. Singh ¹⁵, V.K. Singh ¹³⁵, V. Singhal ¹³⁵, T. Sinha ⁹⁹,
 B. Sitar ¹³, M. Sitta ^{133,56}, T.B. Skaali¹⁹, G. Skorodumovs ⁹⁴, N. Smirnov ¹³⁸, R.J.M. Snellings ⁵⁹,
 E.H. Solheim ¹⁹, J. Song ¹⁶, C. Sonnabend ^{32,97}, J.M. Sonneveld ⁸⁴, F. Soramel ²⁷,
 A.B. Soto-hernandez ⁸⁸, R. Spijkers ⁸⁴, I. Sputowska ¹⁰⁷, J. Staa ⁷⁵, J. Stachel ⁹⁴, I. Stan ⁶³,
 P.J. Steffanic ¹²², T. Stellhorn¹²⁶, S.F. Stiefelmaier ⁹⁴, D. Stocco ¹⁰³, I. Storehaug ¹⁹, N.J. Strangmann ⁶⁴,
 P. Stratmann ¹²⁶, S. Strazzi ²⁵, A. Sturmiolo ^{30,53}, C.P. Stylianidis⁸⁴, A.A.P. Suaide ¹¹⁰, C. Suire ¹³¹,
 M. Sukhanov ¹⁴¹, M. Suljic ³², R. Sultanov ¹⁴¹, V. Sumberia ⁹¹, S. Sumowidagdo ⁸²,
 M. Szymkowski ¹³⁶, S.F. Taghavi ⁹⁵, G. Taillepied ⁹⁷, J. Takahashi ¹¹¹, G.J. Tambave ⁸⁰, S. Tang ⁶,
 Z. Tang ¹²⁰, J.D. Tapia Takaki ¹¹⁸, N. Tapus¹¹³, L.A. Tarasovicova ¹²⁶, M.G. Tazila ⁴⁵, G.F. Tassielli ³¹,
 A. Tauro ³², A. Tavira García ¹³¹, G. Tejeda Muñoz ⁴⁴, A. Telesca ³², L. Terlizzi ²⁴, C. Terrevoli ⁵⁰,
 S. Thakur ⁴, D. Thomas ¹⁰⁸, A. Tikhonov ¹⁴¹, N. Tiltmann ^{32,126}, A.R. Timmins ¹¹⁶, M. Tkacik¹⁰⁶,
 T. Tkacik ¹⁰⁶, A. Toia ⁶⁴, R. Tokumoto⁹², S. Tomassini²⁵, K. Tomohiro⁹², N. Topilskaya ¹⁴¹, M. Toppi ⁴⁹,
 V.V. Torres ¹⁰³, A.G. Torres Ramos ³¹, A. Trifiro ^{30,53}, T. Triloki⁹⁶, A.S. Triolo ^{32,30,53}, S. Tripathy ³²,
 T. Tripathy ⁴⁷, V. Trubnikov ³, W.H. Trzaska ¹¹⁷, T.P. Trzcinski ¹³⁶, C. Tsolanta¹⁹, R. Tu³⁹,
 A. Tumkin ¹⁴¹, R. Turrisi ⁵⁴, T.S. Tveter ¹⁹, K. Ullaland ²⁰, B. Ulukutlu ⁹⁵, S. Upadhyaya ¹⁰⁷,
 A. Uras ¹²⁸, M. Urioni ¹³⁴, G.L. Usai ²², M. Vala³⁷, N. Valle ⁵⁵, L.V.R. van Doremalen⁵⁹, M. van
 Leeuwen ⁸⁴, C.A. van Veen ⁹⁴, R.J.G. van Weelden ⁸⁴, P. Vande Vyvre ³², D. Varga ⁴⁶, Z. Varga ⁴⁶,
 P. Vargas Torres⁶⁵, M. Vasileiou ⁷⁸, A. Vasiliev ¹⁴¹, O. Vázquez Doce ⁴⁹, O. Vazquez Rueda ¹¹⁶,
 V. Vechernin ¹⁴¹, E. Vercellin ²⁴, S. Vergara Limón⁴⁴, R. Verma⁴⁷, L. Vermunt ⁹⁷, R. Vértesi ⁴⁶,
 M. Verweij ⁵⁹, L. Vickovic³³, Z. Vilakazi¹²³, O. Villalobos Baillie ¹⁰⁰, A. Villani ²³, A. Vinogradov ¹⁴¹,
 T. Virgili ²⁸, M.M.O. Virta ¹¹⁷, A. Vodopyanov ¹⁴², B. Volkel ³², M.A. Völkl ⁹⁴, S.A. Voloshin ¹³⁷,

G. Volpe ³¹, B. von Haller ³², I. Vorobyev ³², N. Vozniuk ¹⁴¹, J. Vrláková ³⁷, J. Wan³⁹, C. Wang ³⁹, D. Wang³⁹, Y. Wang ³⁹, Y. Wang ⁶, A. Wegrzynek ³², F.T. Weiglhofer³⁸, S.C. Wenzel ³², J.P. Wessels ¹²⁶, J. Wiechula ⁶⁴, J. Wikne ¹⁹, G. Wilk ⁷⁹, J. Wilkinson ⁹⁷, G.A. Willems ¹²⁶, B. Windelband ⁹⁴, M. Winn ¹³⁰, J.R. Wright ¹⁰⁸, W. Wu³⁹, Y. Wu ¹²⁰, Z. Xiong¹²⁰, R. Xu ⁶, A. Yadav ⁴², A.K. Yadav ¹³⁵, Y. Yamaguchi ⁹², S. Yang²⁰, S. Yano ⁹², E.R. Yeats¹⁸, Z. Yin ⁶, I.-K. Yoo ¹⁶, J.H. Yoon ⁵⁸, H. Yu¹², S. Yuan²⁰, A. Yuncu ⁹⁴, V. Zaccolo ²³, C. Zampolli ³², M. Zang⁶, F. Zanone ⁹⁴, N. Zardoshti ³², A. Zarochentsev ¹⁴¹, P. Závada ⁶², N. Zaviyalov¹⁴¹, M. Zhalov ¹⁴¹, B. Zhang ^{94,6}, C. Zhang ¹³⁰, L. Zhang ³⁹, M. Zhang^{127,6}, S. Zhang ³⁹, X. Zhang ⁶, Y. Zhang¹²⁰, Z. Zhang ⁶, M. Zhao ¹⁰, V. Zhrebchevskii ¹⁴¹, Y. Zhi¹⁰, D. Zhou ⁶, Y. Zhou ⁸³, J. Zhu ^{54,6}, S. Zhu¹²⁰, Y. Zhu⁶, S.C. Zugravel ⁵⁶, N. Zurlo ^{134,55}

Affiliation Notes

^I Deceased

^{II} Also at: Max-Planck-Institut für Physik, Munich, Germany

^{III} Also at: Italian National Agency for New Technologies, Energy and Sustainable Economic Development (ENEA), Bologna, Italy

^{IV} Also at: Dipartimento DET del Politecnico di Torino, Turin, Italy

^V Also at: Yildiz Technical University, Istanbul, Türkiye

^{VI} Also at: Department of Applied Physics, Aligarh Muslim University, Aligarh, India

^{VII} Also at: Institute of Theoretical Physics, University of Wrocław, Poland

^{VIII} Also at: An institution covered by a cooperation agreement with CERN

Collaboration Institutes

¹ A.I. Alikhanyan National Science Laboratory (Yerevan Physics Institute) Foundation, Yerevan, Armenia

² AGH University of Krakow, Cracow, Poland

³ Bogolyubov Institute for Theoretical Physics, National Academy of Sciences of Ukraine, Kiev, Ukraine

⁴ Bose Institute, Department of Physics and Centre for Astroparticle Physics and Space Science (CAPSS), Kolkata, India

⁵ California Polytechnic State University, San Luis Obispo, California, United States

⁶ Central China Normal University, Wuhan, China

⁷ Centro de Aplicaciones Tecnológicas y Desarrollo Nuclear (CEADEN), Havana, Cuba

⁸ Centro de Investigación y de Estudios Avanzados (CINVESTAV), Mexico City and Mérida, Mexico

⁹ Chicago State University, Chicago, Illinois, United States

¹⁰ China Institute of Atomic Energy, Beijing, China

¹¹ China University of Geosciences, Wuhan, China

¹² Chungbuk National University, Cheongju, Republic of Korea

¹³ Comenius University Bratislava, Faculty of Mathematics, Physics and Informatics, Bratislava, Slovak Republic

¹⁴ Creighton University, Omaha, Nebraska, United States

¹⁵ Department of Physics, Aligarh Muslim University, Aligarh, India

¹⁶ Department of Physics, Pusan National University, Pusan, Republic of Korea

¹⁷ Department of Physics, Sejong University, Seoul, Republic of Korea

¹⁸ Department of Physics, University of California, Berkeley, California, United States

¹⁹ Department of Physics, University of Oslo, Oslo, Norway

²⁰ Department of Physics and Technology, University of Bergen, Bergen, Norway

²¹ Dipartimento di Fisica, Università di Pavia, Pavia, Italy

²² Dipartimento di Fisica dell'Università and Sezione INFN, Cagliari, Italy

²³ Dipartimento di Fisica dell'Università and Sezione INFN, Trieste, Italy

²⁴ Dipartimento di Fisica dell'Università and Sezione INFN, Turin, Italy

²⁵ Dipartimento di Fisica e Astronomia dell'Università and Sezione INFN, Bologna, Italy

²⁶ Dipartimento di Fisica e Astronomia dell'Università and Sezione INFN, Catania, Italy

²⁷ Dipartimento di Fisica e Astronomia dell'Università and Sezione INFN, Padova, Italy

²⁸ Dipartimento di Fisica 'E.R. Caianiello' dell'Università and Gruppo Collegato INFN, Salerno, Italy

²⁹ Dipartimento DISAT del Politecnico and Sezione INFN, Turin, Italy

³⁰ Dipartimento di Scienze MIFT, Università di Messina, Messina, Italy

- ³¹ Dipartimento Interateneo di Fisica ‘M. Merlin’ and Sezione INFN, Bari, Italy
- ³² European Organization for Nuclear Research (CERN), Geneva, Switzerland
- ³³ Faculty of Electrical Engineering, Mechanical Engineering and Naval Architecture, University of Split, Split, Croatia
- ³⁴ Faculty of Engineering and Science, Western Norway University of Applied Sciences, Bergen, Norway
- ³⁵ Faculty of Nuclear Sciences and Physical Engineering, Czech Technical University in Prague, Prague, Czech Republic
- ³⁶ Faculty of Physics, Sofia University, Sofia, Bulgaria
- ³⁷ Faculty of Science, P.J. Šafárik University, Košice, Slovak Republic
- ³⁸ Frankfurt Institute for Advanced Studies, Johann Wolfgang Goethe-Universität Frankfurt, Frankfurt, Germany
- ³⁹ Fudan University, Shanghai, China
- ⁴⁰ Gangneung-Wonju National University, Gangneung, Republic of Korea
- ⁴¹ Gauhati University, Department of Physics, Guwahati, India
- ⁴² Helmholtz-Institut für Strahlen- und Kernphysik, Rheinische Friedrich-Wilhelms-Universität Bonn, Bonn, Germany
- ⁴³ Helsinki Institute of Physics (HIP), Helsinki, Finland
- ⁴⁴ High Energy Physics Group, Universidad Autónoma de Puebla, Puebla, Mexico
- ⁴⁵ Horia Hulubei National Institute of Physics and Nuclear Engineering, Bucharest, Romania
- ⁴⁶ HUN-REN Wigner Research Centre for Physics, Budapest, Hungary
- ⁴⁷ Indian Institute of Technology Bombay (IIT), Mumbai, India
- ⁴⁸ Indian Institute of Technology Indore, Indore, India
- ⁴⁹ INFN, Laboratori Nazionali di Frascati, Frascati, Italy
- ⁵⁰ INFN, Sezione di Bari, Bari, Italy
- ⁵¹ INFN, Sezione di Bologna, Bologna, Italy
- ⁵² INFN, Sezione di Cagliari, Cagliari, Italy
- ⁵³ INFN, Sezione di Catania, Catania, Italy
- ⁵⁴ INFN, Sezione di Padova, Padova, Italy
- ⁵⁵ INFN, Sezione di Pavia, Pavia, Italy
- ⁵⁶ INFN, Sezione di Torino, Turin, Italy
- ⁵⁷ INFN, Sezione di Trieste, Trieste, Italy
- ⁵⁸ Inha University, Incheon, Republic of Korea
- ⁵⁹ Institute for Gravitational and Subatomic Physics (GRASP), Utrecht University/Nikhef, Utrecht, Netherlands
- ⁶⁰ Institute of Experimental Physics, Slovak Academy of Sciences, Košice, Slovak Republic
- ⁶¹ Institute of Physics, Homi Bhabha National Institute, Bhubaneswar, India
- ⁶² Institute of Physics of the Czech Academy of Sciences, Prague, Czech Republic
- ⁶³ Institute of Space Science (ISS), Bucharest, Romania
- ⁶⁴ Institut für Kernphysik, Johann Wolfgang Goethe-Universität Frankfurt, Frankfurt, Germany
- ⁶⁵ Instituto de Ciencias Nucleares, Universidad Nacional Autónoma de México, Mexico City, Mexico
- ⁶⁶ Instituto de Física, Universidade Federal do Rio Grande do Sul (UFRGS), Porto Alegre, Brazil
- ⁶⁷ Instituto de Física, Universidad Nacional Autónoma de México, Mexico City, Mexico
- ⁶⁸ iThemba LABS, National Research Foundation, Somerset West, South Africa
- ⁶⁹ Jeonbuk National University, Jeonju, Republic of Korea
- ⁷⁰ Johann-Wolfgang-Goethe Universität Frankfurt Institut für Informatik, Fachbereich Informatik und Mathematik, Frankfurt, Germany
- ⁷¹ Korea Institute of Science and Technology Information, Daejeon, Republic of Korea
- ⁷² KTO Karatay University, Konya, Turkey
- ⁷³ Laboratoire de Physique Subatomique et de Cosmologie, Université Grenoble-Alpes, CNRS-IN2P3, Grenoble, France
- ⁷⁴ Lawrence Berkeley National Laboratory, Berkeley, California, United States
- ⁷⁵ Lund University Department of Physics, Division of Particle Physics, Lund, Sweden
- ⁷⁶ Nagasaki Institute of Applied Science, Nagasaki, Japan
- ⁷⁷ Nara Women’s University (NWU), Nara, Japan
- ⁷⁸ National and Kapodistrian University of Athens, School of Science, Department of Physics, Athens, Greece
- ⁷⁹ National Centre for Nuclear Research, Warsaw, Poland
- ⁸⁰ National Institute of Science Education and Research, Homi Bhabha National Institute, Jatni, India
- ⁸¹ National Nuclear Research Center, Baku, Azerbaijan

- 82 National Research and Innovation Agency - BRIN, Jakarta, Indonesia
- 83 Niels Bohr Institute, University of Copenhagen, Copenhagen, Denmark
- 84 Nikhef, National institute for subatomic physics, Amsterdam, Netherlands
- 85 Nuclear Physics Group, STFC Daresbury Laboratory, Daresbury, United Kingdom
- 86 Nuclear Physics Institute of the Czech Academy of Sciences, Husinec-Řež, Czech Republic
- 87 Oak Ridge National Laboratory, Oak Ridge, Tennessee, United States
- 88 Ohio State University, Columbus, Ohio, United States
- 89 Physics department, Faculty of science, University of Zagreb, Zagreb, Croatia
- 90 Physics Department, Panjab University, Chandigarh, India
- 91 Physics Department, University of Jammu, Jammu, India
- 92 Physics Program and International Institute for Sustainability with Knotted Chiral Meta Matter (SKCM2), Hiroshima University, Hiroshima, Japan
- 93 Physikalisches Institut, Eberhard-Karls-Universität Tübingen, Tübingen, Germany
- 94 Physikalisches Institut, Ruprecht-Karls-Universität Heidelberg, Heidelberg, Germany
- 95 Physik Department, Technische Universität München, Munich, Germany
- 96 Politecnico di Bari and Sezione INFN, Bari, Italy
- 97 Research Division and ExtreMe Matter Institute EMMI, GSI Helmholtzzentrum für Schwerionenforschung GmbH, Darmstadt, Germany
- 98 Saga University, Saga, Japan
- 99 Saha Institute of Nuclear Physics, Homi Bhabha National Institute, Kolkata, India
- 100 School of Physics and Astronomy, University of Birmingham, Birmingham, United Kingdom
- 101 Sección Física, Departamento de Ciencias, Pontificia Universidad Católica del Perú, Lima, Peru
- 102 Stefan Meyer Institut für Subatomare Physik (SMI), Vienna, Austria
- 103 SUBATECH, IMT Atlantique, Nantes Université, CNRS-IN2P3, Nantes, France
- 104 Sungkyunkwan University, Suwon City, Republic of Korea
- 105 Suranaree University of Technology, Nakhon Ratchasima, Thailand
- 106 Technical University of Košice, Košice, Slovak Republic
- 107 The Henryk Niewodniczanski Institute of Nuclear Physics, Polish Academy of Sciences, Cracow, Poland
- 108 The University of Texas at Austin, Austin, Texas, United States
- 109 Universidad Autónoma de Sinaloa, Culiacán, Mexico
- 110 Universidade de São Paulo (USP), São Paulo, Brazil
- 111 Universidade Estadual de Campinas (UNICAMP), Campinas, Brazil
- 112 Universidade Federal do ABC, Santo Andre, Brazil
- 113 Universitatea Nationala de Stiinta si Tehnologie Politehnica Bucuresti, Bucharest, Romania
- 114 University of Cape Town, Cape Town, South Africa
- 115 University of Derby, Derby, United Kingdom
- 116 University of Houston, Houston, Texas, United States
- 117 University of Jyväskylä, Jyväskylä, Finland
- 118 University of Kansas, Lawrence, Kansas, United States
- 119 University of Liverpool, Liverpool, United Kingdom
- 120 University of Science and Technology of China, Hefei, China
- 121 University of South-Eastern Norway, Kongsberg, Norway
- 122 University of Tennessee, Knoxville, Tennessee, United States
- 123 University of the Witwatersrand, Johannesburg, South Africa
- 124 University of Tokyo, Tokyo, Japan
- 125 University of Tsukuba, Tsukuba, Japan
- 126 Universität Münster, Institut für Kernphysik, Münster, Germany
- 127 Université Clermont Auvergne, CNRS/IN2P3, LPC, Clermont-Ferrand, France
- 128 Université de Lyon, CNRS/IN2P3, Institut de Physique des 2 Infinis de Lyon, Lyon, France
- 129 Université de Strasbourg, CNRS, IPHC UMR 7178, F-67000 Strasbourg, France, Strasbourg, France
- 130 Université Paris-Saclay, Centre d'Etudes de Saclay (CEA), IRFU, Département de Physique Nucléaire (DPhN), Saclay, France
- 131 Université Paris-Saclay, CNRS/IN2P3, IJCLab, Orsay, France
- 132 Università degli Studi di Foggia, Foggia, Italy
- 133 Università del Piemonte Orientale, Vercelli, Italy
- 134 Università di Brescia, Brescia, Italy

- ¹³⁵ Variable Energy Cyclotron Centre, Homi Bhabha National Institute, Kolkata, India
¹³⁶ Warsaw University of Technology, Warsaw, Poland
¹³⁷ Wayne State University, Detroit, Michigan, United States
¹³⁸ Yale University, New Haven, Connecticut, United States
¹³⁹ Yonsei University, Seoul, Republic of Korea
¹⁴⁰ Zentrum für Technologie und Transfer (ZTT), Worms, Germany
¹⁴¹ Affiliated with an institute covered by a cooperation agreement with CERN
¹⁴² Affiliated with an international laboratory covered by a cooperation agreement with CERN.